Flexoelectric Effect at the Nanoscale

17

Lele L. Ma, Weijin J. Chen, and Yue Zheng

Contents

L. L. Ma · Y. Zheng (✉)
State Key Laboratory of Optoelectronic Materials and Technologies, Sun Yat-sen University, Guangzhou, China

Micro&Nano Physics and Mechanics Research Laboratory, School of Physics, Sun Yat-sen University, Guangzhou, China

School of Engineering, Sun Yat-sen University, Guangzhou, China
e-mail: zhengy35@mail.sysu.edu.cn

W. J. Chen
State Key Laboratory of Optoelectronic Materials and Technologies, Sun Yat-sen University, Guangzhou, China

Micro&Nano Physics and Mechanics Research Laboratory, School of Physics, Sun Yat-sen University, Guangzhou, China
e-mail: chenweijin@mail.sysu.edu.cn

C.-H. Hsueh et al. (eds.), *Handbook of Mechanics of Materials*,
https://doi.org/10.1007/978-981-10-6884-3_18

Abstract

Flexoelectric effect is a universal electromechanical coupling effect in solids. Nevertheless, it has been ignored for a long time, due to the usual small strain gradients in materials. The case is different for nanomaterials, where strain gradients can usually reach to the order of 10^6 m^{-1}. Moreover, as the flexoelectric effect scales with dielectric susceptibility, it can be much more apparent in materials with higher dielectric constants, such as ferroelectrics. Due to this reason, increasing attention has been attracted on the flexoelectric effect in nanomaterials (with ferroelectrics as the representatives) during the past few years. The large flexoelectric effect in nanomaterials not only makes them promising candidates to design novel electromechanical nanodevices but also strongly modifies many material properties such as polarization switching, ferroelectric domains and domain walls, polarization-mediated electronic transport effects, etc. Focusing on flexoelectric effect at the nanoscale and with ferroelectrics as the representatives, this chapter aims to provide an overview of this rapidly growing field, including the theoretical models and experimental characterization methods of flexoelectric effect, the recent important progress of flexoelectric effect, as well as the potential applications.

Keywords

Flexoelectricity · Ferroelectric · Nanoscale · Strain gradient · Polarization

1 Introduction

Flexoelectric effect, also called flexoelectricity or nonlocal piezoelectric effect, describes the linear electromechanical coupling between electrical polarization and strain gradients in materials. Concretely speaking, it characterizes the induced polarization by inhomogeneous strain or the strain resulted from the polarization inhomogeneity, where the former corresponds to the direct flexoelectric effect and the latter corresponds to the converse flexoelectric effect. Flexoelectricity manifests itself in a variety of materials, such as solid dielectrics, liquid crystals and biological systems, etc. The physical mechanisms in different kinds of materials can be quite different. Here the discussions are mainly confined in the flexoelectricity of solids.

When we talk about electromechanical couplings, it is inevitable to mention piezoelectricity, which characterizes the linear coupling between polarization and homogeneous strain. A big difference between piezoelectricity and flexoelectricity is their different requirements on the symmetry of materials. Piezoelectricity can only be found in 20 point groups which are non-centrosymmetric, for homogeneous strain cannot change the symmetry of materials. In contrast, with inhomogeneous strain or strain gradients, the symmetry of materials will be broken, which results in the

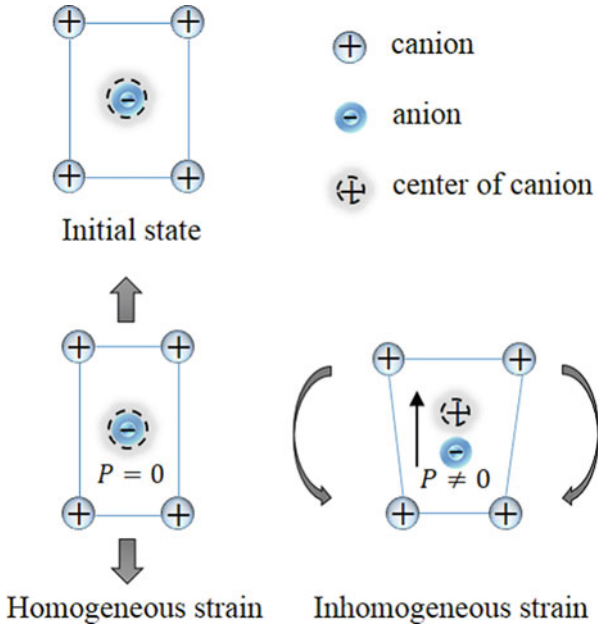

Fig. 1 Schematic of the effect of homogeneous and inhomogeneous strain on the symmetry of centrosymmetric lattice. It can be seen that the homogeneous strain has no effect on the lattice symmetry and introduces no polarization, but the inhomogeneous strain or strain gradient does break the lattice symmetry and induces net polarization in the centrosymmetric lattice

generation of polarization and enables the universality of flexoelectricity in the whole 32 point groups (see Fig. 1). So compared with piezoelectricity, flexoelectricity is more general and it broadens the scope of candidate materials possessing desired electromechanical behaviors. The flexoelectric effect in solids was predicted theoretically in the 1950s [1]. In 1964, Kogan [2] proposed a phenomenological description for this effect firstly and estimated the order of magnitude of the flexoelectric coefficients. In 1968, Mindlin [3] first introduced polarization gradient term into the continuum theory. At the same year, Bursian [4] experimentally observed the bending of a thin $BaTiO_3$ (BTO) film due to polarization, which is the beginning of investigating converse flexoelectric effect, i.e., the linear coupling between polarization gradient and strain. In 1974, Bursian [5] used the term "nonlocal piezoelectric effect," and the terminology was substituted by "flexoelectric effect" in 1981 by Indenbom [6]. Then Tagantsev [7] presented a phenomenological description systematically on flexoelectricity and made the first attempt to investigate this effect microscopically. The derived results in his work showed that the flexoelectric effect could be divided into several contributions and the bulk flexoelectric coefficients are scaling with the dielectric susceptibility proportionally. Toward applications, Fousek et al. [8] proposed the idea of "flexoelectricity-based piezoelectric composites" which have no piezoelectric constituents in 1999. Though these achievements have been made, there have been only a few interests in this area until at the beginning of the new century.

The situation changed after a series of experimental works conducted by Ma and Cross et al. [9]. They determined the flexoelectric coefficients of several ferroelectric ceramics and confirmed the susceptibility dependence of the flexoelectric coefficients, but the obtained values of the coefficients in some materials were much larger than the preceding theoretical estimations. Then Zubko et al. [10] experimentally investigated the flexoelectricity of $SrTiO_3$ (STO) single crystals and obtained its all three flexoelectric coefficients for the first time. Some theoretical works also began to take flexoelectric effect into consideration, and flexoelectricity was drawing more and more attentions. During the past decade, flexoelectric effect has aroused great interests, and the investigations have been broadened to several aspects. These include (a) the theoretical calculation of flexoelectric coefficients both phenomenologically and microscopically as well as those by the first-principle methods, (b) the experimental determination of flexoelectric coefficients, (c) the manifestation of flexoelectric effect in the physical properties of materials, (d) the explanation of some confusing but novel phenomena by taking this effect into consideration, (e) the innovative applications and device design based on flexoelectricity and (f) the construction of continuum theories involving the flexoelectric term, etc.

The ignorance of flexoelectricity in its early years was mainly due to the relative weakness of the effect in bulk materials with common scales, for the order of magnitude of the flexoelectric coefficients are estimated as $\sim e/a$ (10^{-9}C/m), where e is the electron charge and a is the lattice constant. Accompanying the progress in material science and technology, however, the dimensions of materials scale down, and the strain gradients obtained can be much larger. Especially, with the dimensions of materials down to nanoscale, the flexoelectric effect can be quite significant and even plays a dominant role. Moreover, as the flexoelectric coefficients scale with dielectric susceptibility, the effect can be much more apparent in materials with higher dielectric constants.

In this chapter, a review on the flexoelectric effect at the nanoscale, with ferroelectrics as the representatives, will be presented. Ferroelectrics are typical materials exhibiting high dielectric constants; thus, they are promising prototypes for the investigations of nontrivial flexoelectricity. They also exhibit a wide range of fascinating properties such as polarization switching, ferroelectric domains and domain walls, polarization-mediated electronic transport effects, etc. Importantly, many properties of ferroelectrics show strong size-dependence, due to the collective feature of the ferroelectricity. In combination with the flexoelectric effect and size effects, nanoscale ferroelectrics could present abundant phenomena and introduce interesting applications. In the following, Section 2 builds up a thermodynamic model involving the bulk static flexoelectricity in nano-ferroelectrics and introduces Tagantsev's microscopic rigid ion model. Then the theoretical works about the calculations of the flexoelectric coefficients are briefly retrospected, and the size effects of flexoelectricity are discussed. The experimental characterization of flexoelectricity is introduced in Sect. 3. Section 4 involves the influence of flexoelectricity on material properties and its effects on domains and domain walls. Section 5 introduces the applications of flexoelectricity, and a conclusion is made in Sect. 6.

2 Theoretical Descriptions of Flexoelectric Effect

2.1 Thermodynamic Model of Ferroelectrics with Flexoelectricity

The flexoelectricity-induced polarization can be written as

$$P_l = \mu_{ijkl} \frac{\partial \varepsilon_{ij}}{\partial x_k} \tag{1}$$

where ε_{ij} is the strain tensor and μ_{ijkl} is the flexoelectric tensor. Einstein summation convention is assumed hereafter with the dummy index running from 1 to 3. The flexoelectric tensor is a fourth-rank tensor which guarantees the existence of flexoelectricity in all crystals with any symmetry mathematically. It has 54 independent components for most general cases. For cubic crystals, it has only three independent components known as the longitudinal coefficient μ_{11}, transverse coefficient μ_{12}, and shear coefficients μ_{44}.

To characterize flexoelectricity (including both the direct and converse effect), the total free energy density of a ferroelectric system should be supplemented by adding the linear coupling term between the polarization and strain gradient and the term between the strain and polarization gradient. This term is denoted as f_{flexo}, which represents the flexoelectric coupling energy density

$$\begin{aligned} f_{\text{flexo}}(P_i, \varepsilon_{ij}, \nabla P_i, \nabla \varepsilon_{ij}) &= -f^{(1)}_{ijkl} P_k \frac{\partial \varepsilon_{ij}}{\partial x_l} - f^{(2)}_{ijkl} \varepsilon_{ij} \frac{\partial P_k}{\partial x_l} \\ &= -\frac{f^{(1)}_{ijkl} + f^{(2)}_{ijkl}}{2} \frac{\partial (P_k \varepsilon_{ij})}{\partial x_l} - \frac{f^{(1)}_{ijkl} - f^{(2)}_{ijkl}}{2} \left(P_k \frac{\partial \varepsilon_{ij}}{\partial x_l} - \varepsilon_{ij} \frac{\partial P_k}{\partial x_l} \right) \end{aligned} \tag{2}$$

where $f^{(1)}_{ijkl}$ and $f^{(2)}_{ijkl}$ are the coupling coefficients. The volume integral of the first term on the right-hand side can be transformed to a surface integral, and it makes no contribution in the energy minimization process. Therefore, the flexoelectric coupling energy density can be written as the Lifshitz invariant

$$f_{\text{flexo}}(P_i, \varepsilon_{ij}, \nabla P_i, \nabla \varepsilon_{ij}) = \frac{1}{2} f_{ijkl} \left(\varepsilon_{ij} \frac{\partial P_k}{\partial x_l} - P_k \frac{\partial \varepsilon_{ij}}{\partial x_l} \right) \tag{3}$$

where $f_{ijkl} = f^{(1)}_{ijkl} - f^{(2)}_{ijkl}$ is the bulk flexoelectric coupling coefficients and it has the same symmetry with μ_{ijkl}.

The total free energy of ferroelectric system can be expressed as a function of polarization P, electric filed E, and strain ε_{ij},

$$\begin{aligned} F &= F_{\text{Land}} + F_{\text{elas}} + F_{\text{grad}} + F_{\text{elec}} + F_{\text{flexo}} + F_{\text{surf}} \\ &= \int \left(f_{\text{Land}} + f_{\text{elas}} + f_{\text{grad}} + f_{\text{elec}} + f_{\text{flexo}} \right) \mathrm{d}V + \int f_{\text{surf}} \mathrm{d}S \end{aligned} \tag{4}$$

where F_{Land}, F_{elas}, F_{grad}, F_{elec}, F_{flexo} and F_{surf} are the Landau free energy, elastic energy, gradient energy, electric energy, flexoelectric coupling energy, and surface energy, respectively, and f_{Land}, f_{elas}, f_{grad}, f_{elec}, f_{flexo} and f_{surf} are the corresponding energy densities.

For a typical perovskite ferroelectric material such as $BaTiO_3$, the Landau free energy density can be written as an eighth-order polynomial:

$$\begin{aligned} f_{\text{Land}}(P_i) = {} & a_1\left({P_1}^2+{P_2}^2+{P_3}^2\right)+a_{11}\left({P_1}^4+{P_2}^4+{P_3}^4\right) \\ & +a_{12}\left({P_1}^2{P_2}^2+{P_1}^2{P_3}^2+{P_2}^2{P_3}^2\right)+a_{111}\left({P_1}^6+{P_2}^6+{P_3}^6\right) \\ & +a_{112}\left[{P_1}^2\left({P_2}^4+{P_3}^4\right)+{P_2}^2\left({P_1}^4+{P_3}^4\right)+{P_3}^2\left({P_1}^4+{P_2}^4\right)\right] \\ & +a_{123}{P_1}^2{P_2}^2{P_3}^2+a_{1111}\left({P_1}^8+{P_2}^8+{P_3}^8\right) \\ & +a_{1112}\left[{P_1}^6\left({P_2}^2+{P_3}^2\right)+{P_2}^6\left({P_1}^2+{P_3}^2\right)+{P_3}^6\left({P_1}^2+{P_2}^2\right)\right] \\ & +a_{1122}\left({P_1}^4{P_2}^4+{P_1}^4{P_3}^4+{P_2}^4{P_3}^4\right) \\ & +a_{1123}\left({P_1}^4{P_2}^2{P_3}^2+{P_2}^4{P_1}^2{P_3}^2+{P_3}^4{P_1}^2{P_2}^2\right) \end{aligned} \tag{5}$$

where a_1, a_{11}, a_{12}, a_{111}, a_{112}, a_{123}, a_{1111}, a_{1112}, a_{1122} and a_{1123} are the phenomenological coefficients.

With the existence of eigenstrain ${\varepsilon_{ij}}^0$ caused by electrostriction, the elastic energy density of the system can be written as

$$\begin{aligned} f_{\text{elas}}\left(P_i,\varepsilon_{ij}\right) = {} & \frac{1}{2}C_{ijkl}\left(\varepsilon_{ij}-{\varepsilon_{ij}}^0\right)\left(\varepsilon_{kl}-{\varepsilon_{kl}}^0\right) \\ = {} & \frac{1}{2}C_{11}\left({\varepsilon_{11}}^2+{\varepsilon_{22}}^2+{\varepsilon_{33}}^2\right)+C_{12}\left(\varepsilon_{11}\varepsilon_{22}+\varepsilon_{11}\varepsilon_{33}+\varepsilon_{22}\varepsilon_{33}\right) \\ & +2C_{44}\left({\varepsilon_{12}}^2+{\varepsilon_{13}}^2+{\varepsilon_{23}}^2\right)+\beta_{11}\left({P_1}^4+{P_2}^4+{P_3}^4\right) \\ & +\beta_{12}\left({P_1}^2{P_2}^2+{P_2}^2{P_3}^2+{P_3}^2{P_1}^2\right)-\varepsilon_{11}\left[q_{11}{P_1}^2+q_{12}\left({P_2}^2+{P_3}^2\right)\right] \\ & -\varepsilon_{22}\left[q_{11}{P_2}^2+q_{12}\left({P_1}^2+{P_3}^2\right)\right]-\varepsilon_{33}\left[q_{11}{P_3}^2+q_{12}\left({P_1}^2+{P_2}^2\right)\right] \\ & -2q_{44}\left(\varepsilon_{12}P_1P_2+\varepsilon_{13}P_1P_3+\varepsilon_{23}P_2P_3\right) \end{aligned} \tag{6}$$

with

$$\beta_{11}=\frac{1}{2}C_{11}\left({Q_{11}}^2+2{Q_{12}}^2\right)+C_{12}Q_{12}\left(2Q_{11}+Q_{12}\right)$$

$$\beta_{12}=C_{11}Q_{12}\left(2Q_{11}+Q_{12}\right)+C_{12}\left({Q_{11}}^2+3{Q_{12}}^2+2Q_{11}Q_{12}\right)+2C_{44}{Q_{44}}^2$$

$$q_{11}=C_{11}Q_{11}+2C_{12}Q_{12}$$

$$q_{12}=C_{11}Q_{12}+C_{12}Q_{11}+C_{12}Q_{12}$$

$$q_{44}=2C_{44}Q_{44}$$

where C_{11}, C_{12} and C_{44} are the elastic moduli and Q_{11}, Q_{12} and Q_{44} are the electrostrictive coefficients.

The gradient energy density can be written as

$$f_{\text{grad}}\left(\nabla_j P_i, \nabla_k \varepsilon_{ij}\right) = \frac{1}{2} g_{ijkl} P_{i,j} P_{k,l} + \frac{1}{2} w_{ijklmn} \varepsilon_{ij,k} \varepsilon_{lm,n} \tag{7}$$

where g_{ijkl} and w_{ijklmn} are the gradient coefficients. The second term on the right-hand side of Eq. (7) appears to guarantee a smooth distribution of the order parameter in the presence of flexoelectric coupling term. Under the condition $f_{klmn}^2 < g_{ijkl} C_{ijmn}$, this term can be neglected, and the gradient energy can be simplified as

$$\begin{aligned} f_{\text{grad}}\left(\nabla_j P_i, \nabla_k \varepsilon_{ij}\right) = {} & \frac{1}{2} G_{11}\left[\left(\frac{\partial P_1}{\partial x_1}\right)^2 + \left(\frac{\partial P_2}{\partial x_2}\right)^2 + \left(\frac{\partial P_3}{\partial x_3}\right)^2\right] \\ & + G_{12}\left(\frac{\partial P_1}{\partial x_1}\frac{\partial P_2}{\partial x_2} + \frac{\partial P_1}{\partial x_1}\frac{\partial P_3}{\partial x_3} + \frac{\partial P_2}{\partial x_2}\frac{\partial P_3}{\partial x_3}\right) \\ & + \frac{1}{2} G_{44}\left[\left(\frac{\partial P_1}{\partial x_2} + \frac{\partial P_2}{\partial x_1}\right)^2 + \left(\frac{\partial P_1}{\partial x_3} + \frac{\partial P_3}{\partial x_1}\right)^2 + \left(\frac{\partial P_2}{\partial x_3} + \frac{\partial P_3}{\partial x_2}\right)^2\right] \\ & + \frac{1}{2} G_{44}{}'\left[\left(\frac{\partial P_1}{\partial x_2} - \frac{\partial P_2}{\partial x_1}\right)^2 + \left(\frac{\partial P_1}{\partial x_3} - \frac{\partial P_3}{\partial x_1}\right)^2 + \left(\frac{\partial P_2}{\partial x_3} - \frac{\partial P_3}{\partial x_2}\right)^2\right] \end{aligned} \tag{8}$$

The electric energy density is

$$f_{\text{elec}} = -P_i E_i - \frac{1}{2}\epsilon_b E_i E_i = -(P_1 E_1 + P_2 E_2 + P_3 E_3) - \frac{1}{2}\epsilon_b (E_1^2 + E_2^2 + E_3^2) \tag{9}$$

where ϵ_b is the background dielectric coefficient.

The flexoelectric coupling energy density is

$$\begin{aligned} & f_{\text{flexo}}\left(P_i, \varepsilon_{ij}, \nabla P_i, \nabla \varepsilon_{ij}\right) = \frac{1}{2} f_{ijkl}\left(\varepsilon_{ij}\frac{\partial P_k}{\partial x_l} - P_k \frac{\partial \varepsilon_{ij}}{\partial x_l}\right) \\ & = \left[\frac{1}{2} f_{11}\varepsilon_{11} + \frac{1}{2} f_{12}(\varepsilon_{22} + \varepsilon_{33})\right]\frac{\partial P_1}{\partial x_1} + \left[\frac{1}{2} f_{11}\varepsilon_{22} + \frac{1}{2} f_{12}(\varepsilon_{11} + \varepsilon_{33})\right]\frac{\partial P_2}{\partial x_2} \\ & + \left[\frac{1}{2} f_{11}\varepsilon_{33} + \frac{1}{2} f_{12}(\varepsilon_{11} + \varepsilon_{22})\right]\frac{\partial P_3}{\partial x_3} \\ & + f_{44}\left[\varepsilon_{12}\left(\frac{\partial P_1}{\partial x_2} + \frac{\partial P_2}{\partial x_1}\right) + \varepsilon_{13}\left(\frac{\partial P_1}{\partial x_3} + \frac{\partial P_3}{\partial x_1}\right) + \varepsilon_{23}\left(\frac{\partial P_2}{\partial x_3} + \frac{\partial P_3}{\partial x_2}\right)\right] \\ & - \left[\frac{1}{2} f_{11}\frac{\partial \varepsilon_{11}}{\partial x_1} + \frac{1}{2} f_{12}\left(\frac{\partial \varepsilon_{22}}{\partial x_1} + \frac{\partial \epsilon_{33}}{\partial x_1}\right) + f_{44}\left(\frac{\partial \varepsilon_{12}}{\partial x_2} + \frac{\partial \varepsilon_{13}}{\partial x_3}\right)\right] P_1 \\ & - \left[\frac{1}{2} f_{11}\frac{\partial \varepsilon_{22}}{\partial x_2} + \frac{1}{2} f_{12}\left(\frac{\partial \varepsilon_{11}}{\partial x_2} + \frac{\partial \varepsilon_{33}}{\partial x_2}\right) + f_{44}\left(\frac{\partial \varepsilon_{12}}{\partial x_1} + \frac{\partial \varepsilon_{23}}{\partial x_3}\right)\right] P_2 \\ & - \left[\frac{1}{2} f_{11}\frac{\partial \varepsilon_{33}}{\partial x_3} + \frac{1}{2} f_{12}\left(\frac{\partial \varepsilon_{11}}{\partial x_3} + \frac{\partial \varepsilon_{22}}{\partial x_3}\right) + f_{44}\left(\frac{\partial \varepsilon_{13}}{\partial x_1} + \frac{\partial \varepsilon_{23}}{\partial x_2}\right)\right] P_3 \end{aligned} \tag{10}$$

where f_{11}, f_{12} and f_{44} are the flexoelectric coupling coefficients.

The surface energy density can be written as

$$f_{\text{surf}}(P_i) = \frac{D_1{}^s P_1{}^2}{2\delta_1{}^{\text{eff}}} + \frac{D_2{}^s P_2{}^2}{2\delta_2{}^{\text{eff}}} + \frac{D_3{}^s P_3{}^2}{2\delta_3{}^{\text{eff}}} \tag{11}$$

with $\delta_i{}^{\text{eff}}$ being the so-called extrapolation length and $D_i{}^s$ being the material coefficients related to the gradient energy coefficients and surface orientations.

To minimize the total free energy F, apply the Euler-Lagrange equations with respect to polarization P_i and strain ε_{ij}, respectively,

$$\frac{\partial F}{\partial P_i} - \frac{\partial}{\partial x_j}\left(\frac{\partial F}{\partial\left(\partial P_i/\partial x_j\right)}\right) = 0 \tag{12a}$$

$$\frac{\partial F}{\partial \varepsilon_{ij}} - \frac{\partial}{\partial x_k}\left(\frac{\partial F}{\partial\left(\partial \varepsilon_{ij}/\partial x_k\right)}\right) = \sigma_{ij} \tag{12b}$$

For simplicity, if just consider the second order of P in the Landau energy density, one can have

$$P_i = \epsilon_0 \chi_{ij}\left(E_j + f_{jmkl}\frac{\partial \varepsilon_{kl}}{\partial x_m}\right) \tag{13}$$

$$\sigma_{ij} = C_{ijkl}\left(\varepsilon_{kl} - \varepsilon_{kl}{}^0\right) + f_{ijkl}\frac{\partial P_k}{\partial x_l} \tag{14}$$

These are the constitutive equations of ferroelectrics considering the flexoelectric effect.

From Eq. (13), it can be seen that the term $f_{jmkl}\,\frac{\partial \epsilon_{kl}}{\partial x_m}$ behaves just like the electric field E_j, so it is defined as the flexoelectric field

$$E_j^f = f_{jmkl}\frac{\partial \varepsilon_{kl}}{\partial x_m} \tag{15}$$

Furthermore, rewrite Eq. (13) by defining $\mu_{ijkl} = \epsilon_0 \chi_{im} f_{mjkl}$, and rewrite Eq. (14) in terms of E by neglecting the term related to the higher-order $\frac{\partial^2 \epsilon_{kl}}{\partial x_i \partial x_j}$,

$$P_i = \epsilon_0 \chi_{ij} E_j + \mu_{ijkl}\frac{\partial \varepsilon_{kl}}{\partial x_j} \tag{16}$$

$$\sigma_{ij} = C_{ijkl}\left(\varepsilon_{kl} - \varepsilon_{kl}{}^0\right) + \mu_{ijkl}\frac{\partial E_k}{\partial x_l} \tag{17}$$

where μ_{ijkl} is the so-called flexoelectric coefficients appearing in Eq. (1). It should be noted that Eq. (17) is only limited to the cases of small strain gradients; for large strain gradients such as in domain walls and interfaces, it is not rigorous because the

neglect of the term $\frac{\partial^2 \epsilon_{kl}}{\partial x_i \partial x_j}$ is not reasonable in such cases. Moreover, with the piezoelectric coupling term involved in the total free energy, the constitutive equations of "general piezoelectricity" can be derived as

$$P_i = \epsilon_0 \chi_{ij} E_j + e_{ijk} \epsilon_{jk} + \mu_{ijkl} \frac{\partial \epsilon_{kl}}{\partial x_j} \tag{18}$$

$$\sigma_{ij} = C_{ijkl}\left(\varepsilon_{kl} - {\varepsilon_{kl}}^0\right) + e_{ijk} E_k + \mu_{ijkl} \frac{\partial E_k}{\partial x_l} \tag{19}$$

with e_{ijk} being the piezoelectric constants.

To investigate the domain structure evolution of ferroelectric system and study the system's responses and physical properties under different boundary conditions, the time-dependent Ginzburg-Landau (TDGL) equations

$$\frac{\partial P_i}{\partial t} = -L \frac{\delta F}{\delta P_i} \tag{20}$$

are commonly employed to describe the evolution of order parameters. For a given ferroelectric system, Eq. (20) should be solved under a set of boundary conditions, i.e., polarization boundary condition, mechanical boundary condition, and electrical boundary condition. The polarization boundary condition can be obtained by varying the total free energy with respect to P_i and equating the variation δF to zero, that is,

$$\frac{\partial f_{\text{surf}}}{\partial P_i} + n_l \left(\frac{\partial f_{\text{bulk}}}{\partial (\partial P_i / \partial x_l)} + \frac{\partial f_{\text{grad}}}{\partial (\partial P_i / \partial x_l)} + \frac{\partial f_{\text{elas}}}{\partial (\partial P_i / \partial x_l)} + \frac{\partial f_{\text{elec}}}{\partial (\partial P_i / \partial x_l)} + \frac{\partial f_{\text{flexo}}}{\partial (\partial P_i / \partial x_l)} \right) \Big|_s = 0 \tag{21}$$

To obtain the mechanical boundary condition in the presence of flexoelectric effect, first substitute the strain ε_{ij} by $\frac{1}{2}\left(u_{i,j} + u_{j,i}\right)$, then vary the total free energy with respect to u_i and equating the variation δF to zero,

$$\frac{\partial f_{\text{surf}}}{\partial u_i} + n_l \left(\frac{\partial f_{\text{bulk}}}{\partial (\partial u_i / \partial x_l)} + \frac{\partial f_{\text{grad}}}{\partial (\partial u_i / \partial x_l)} + \frac{\partial f_{\text{elas}}}{\partial (\partial u_i / \partial x_l)} + \frac{\partial f_{\text{elec}}}{\partial (\partial u_i / \partial x_l)} + \frac{\partial f_{\text{flexo}}}{\partial (\partial u_i / \partial x_l)} \right) \Big|_s = 0 \tag{22}$$

Take a mechanical-free, open-circuit ultrathin ferroelectric film as an example, the equations of boundary conditions at the top and bottom surfaces are

$$\left(\frac{D_i^s}{\delta_i^s} P_i + n_j g_{ijkl} \frac{\partial P_k}{\partial x_l} + n_j \frac{f_{lmij}}{2} \varepsilon_{lm} \right) \Big|_s = 0 \tag{23}$$

$$\left(\sigma_{i3} - \frac{f_{l33l}}{2} + \frac{f_{ij3l}}{2} \frac{\partial P_l}{\partial x_j} \right) \Big|_s = 0 \tag{24}$$

$$\nabla \cdot D|_s = 0 \tag{25}$$

with Eqs. (23), (24), and (25) being the polarization, mechanical, and electrical boundary conditions, respectively. It should be noted that the consideration of flexoelectric effect not only contributes to the TDGL equation but also contributes to the boundary conditions. Nevertheless, in many theoretical works, the modifications of flexoelectric effect on the boundary conditions were ignored. It is still indistinct how much the flexoelectric boundary conditions can influence the domain structure and physical properties of ferroelectric systems. But it is expected that in nanoscale materials, the effect of the flexoelectric boundary conditions should not be neglected not only because of the significance of flexoelectricity but also because of the importance of the surfaces at the nanoscale.

It is noteworthy to point out that the flexoelectricity discussed above is the bulk static flexoelectricity which is somewhat analogous to piezoelectricity. According to Tagantsev's work [7], the dynamic bulk flexoelectric response, for example, the polarization caused by the strain gradients induced by an acoustic wave, can also be derived in a similar way by considering the kinetic energy and can be written as

$$P_i = \epsilon_0 \chi_{ij} E_j + (\mu_{ijkl} + \mu^d_{ijkl}) \frac{\partial \varepsilon_{kl}}{\partial x_j} \tag{26}$$

where μ^d_{ijkl} is the dynamic flexoelectric coefficients which is also proportional to the susceptibility χ_{ij} and is approximately of the same order of magnitude with the bulk static fleoxelectric coefficients. For a system in quasi-static states, the dynamic flexoelectric effect can be ignored.

Moreover, a complete phenomenological description of flexoelectricity for finite samples must include the effects of surfaces or interfaces. A typical example of surface effects that can mimic bulk flexoelectric response is the surface piezoelectricity, where thin piezoelectric layers near the surfaces cause a built-in field across the sample, and the field depends on the strain state of the surfaces. Despite a lack of clear understanding of the surface flexoelectricity, it is believed that it makes an important contribution to the large difference between the experimental flexocoupling coefficients and the theoretical bulk ones. In general, properties near the surface (e.g., bonding and screening environment, surface polarization, surface work function, interface dipole, etc.) should change in response to local strain. As a result, a long-range surface-specific flexoelectric field may arise across the sample due to the strain difference between the surfaces. In this context, besides solving the bulk flexoelectricity, one can include a surface-specific flexoelectric field to the system, for example, for a nanofilm as

$$E_i^{\text{flexo},S} = f^S_{ijkl} \Delta \varepsilon^S_{kl} / h \tag{27}$$

where $\Delta \varepsilon^S_{kl}$ are the components of strain difference between the top and bottom surfaces of the nanofilm, h is the film thickness, and f^S_{ijkl} are the surface-specific flexocoupling coefficients.

It is also noteworthy that recent first-principle calculation has shown that bending strain can induce antiferrodistortive (AFD) displacement associated with the rotation

of oxygen octahedral in ultrathin ferroelectric nanofilms. [11] Interestingly, the bending nanofilm possesses spontaneous polarization (which is absent in flat film) due to the coupling between ferroelectricity and the AFD phase transition. In other words, polarization is induced by strain gradient via the triggering of AFD phase transition. This actually indicates flexoelectricity can be originated from more complex mechanisms. However, a complete phenomenological description of flexoelectricity in nanomaterials taking into account such mechanisms is still lacking.

2.2 Microscopic Theory of Flexoelectric Effect

Though the phenomenological description sheds light on the flexoelectric response of materials and obtains the flexoelectric constitutive equations, it cannot give the magnitude of the flexoelectric coefficients. To estimate the flexoelectric coefficients and uncover the microscopic mechanism of flexoelectricity, various theoretical works have been conducted. In 1964, Kogan [2] first gave the order of magnitude estimation of the flexoelectric coefficients. Following his method, consider a cubic unit cell with lattice constant a, if the strain variation over the interatomic distance equals one, then the strain gradient is $\frac{1}{a}$. With the polarization being of the order of $\frac{ea}{a^3} = ea^{-2}$, the flexoelectric coefficient can be obtained as $\sim \frac{ea^{-2}}{1/a} = \frac{e}{a}$, where e is the absolute value of the electron charge. After Kogan, Tagantsev [7] developed a microscopic description of flexoelectricity based on the "rigid ion" model, which focused on the ionic flexoelectricity and neglected the electronic contribution. Here a brief introduction to this model is given; more details can be found in Reference [7].

Consider a crystal lattice sketched in Fig. 2. Atom B is the nth atom of the lattice, and its jth coordinate is denoted by $R_{n,\,j}$ before deformation. When the lattice is subjected to an inhomogeneous deformation, one can get two kinds of values of the ith components of the displacement of atom B. The first value is an approximation based on the continuum theory and is called the external displacement $w_{n,i}^{\text{ext}}$, set x_j^0 the coordinates of an immobile reference point, then

$$w_{n,i}^{\text{ext}} = \int_{x_j^0}^{R_{n,j}} \frac{\partial u_i}{\partial x_j} \mathrm{d}y_j \tag{28}$$

where $\frac{\partial u_i}{\partial x_j}$ is the so-called external strain. The other value is the real displacement of the atom B according to the discrete nature of the lattice, $w_{n,i}$. The inhomogeneous deformations break the centrosymmetry of the lattice, so $w_{n,i}^{\text{ext}}$ is not coincident with $w_{n,i}$. The difference between $w_{n,i}$ and $w_{n,i}^{\text{ext}}$ is the so-called internal strain $w_{n,i}^{\text{int}}$, and it is proportional to the strain gradient

$$w_{n,i}^{\text{int}} = w_{n,i} - w_{n,i}^{\text{ext}} = N_{n,i}^{jkl} \frac{\partial \varepsilon_{jk}}{\partial x_l} \tag{29}$$

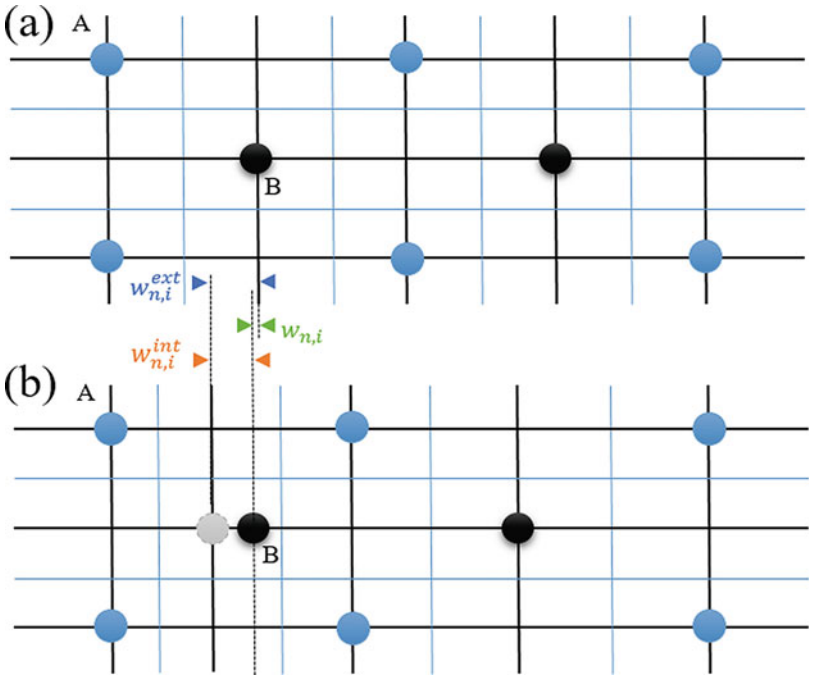

Fig. 2 Schematic of a lattice before **a** and after **b** inhomogeneous deformation

where $N_{n,i}^{jkl}$ can be calculated by the theory of lattice dynamics. If the nth atom has the charge Q_n, the variation of the average polarization induced by the inhomogeneous deformation can be written as

$$\delta P_i = V_{\text{def}}^{-1} \sum_n Q_n \left(R_{n,i} + w_{n,i}\right) - V^{-1} \sum_n Q_n R_{n,i} \tag{30}$$

where V and V_{def} are the volume of the sample before and after deformation, respectively. Substituting Eq. (29) into Eq. (30), one can find the strain gradient induced polarization variation in a unit cell with volume v,

$$\delta P_i = v^{-1} \sum_n Q_n N_{n,i}^{jkl} \frac{\partial \varepsilon_{jk}}{\partial x_l} \tag{31}$$

So the flexoelectric coefficients can be obtained as

$$\mu_{ijkl} = \frac{\delta P_i}{\partial \varepsilon_{jk} / \partial x_l} = v^{-1} \sum_n Q_n N_{n,i}^{jkl} \tag{32}$$

Based on this rigid ion model, Tagantsev [7] divided the flexoelectric effect into four contributions, i.e., static bulk, dynamic bulk, surface piezoelectricity, and

surface flexoelectricity, and the four contributions are generally of the same order of magnitude. As mentioned before, surface piezoelectricity shows its existence in finite samples, the surfaces of which break the symmetry of the system and result in effective piezoelectric layers in vicinity of the surfaces. This contribution is also susceptibility dependent and is independent of the surface/volume ratio. The last contribution, i.e., surface flexoelectricity, is not dependent on the dielectric constant thus relatively insignificant. It should be noted that the surface contribution to the flexoelectric response was challenged by Resta [12], who developed a microscopic description of the electronic contribution to flexoelectricity based on the classical piezoelectric theory.

2.3 The Theoretical Calculations of Flexoelectric Coefficients

To quantify the significance of flexoelectric response, the relatively accurate values of flexoelectric coefficients are needed, not just the order of magnitude estimations. The theoretical calculations of flexoelectric coefficients were conducted just in recent years though the microscopic theories were put forward much earlier. Based on Tagantsev's microscopic model, Maranganti et al. [13] first implemented the calculation of bulk static flexoelectricity. Later, Hong et al. [14] performed the first-principle calculations of longitudinal flexoelectricity using a direct approach. They directly calculated the induced polarization by a given strain profile and extracted the flexoelectric coefficients. The direct methods have the merits of including the extrinsic contributions, such as surface and defect effects. Then Hong and Vanderbilt [15] extended Resta's theory to yield the transverse flexoelectric coefficients and obtained the longitudinal flexoelectric coefficients for a number of materials such as BTO, $PbTiO_3$ (PTO), and STO. Later they developed a more general first-principle theory which included both the electronic and lattice contributions in the context of density-functional calculations [16]. They obtained the relationship of flexoelectric coefficients between the fixed electric field (μ^E_{ijkl}) and fixed electric displacement (μ^D_{mjkl}) boundary conditions:

$$\mu^E_{ijkl} = (\delta_{im} + \chi_{im})\mu^D_{mjkl} \tag{33}$$

where δ_{im} is Kronecker delta. So μ^D_{mjkl} could be seen as a "ground-state bulk property" to calculate the μ^E_{ijkl} at finite temperature by scaling with the dielectric constant. Ponomareva et al. [17] developed an effective Hamiltonian method to study the flexoelectric effect in ferroelectric thin films at finite temperatures and investigated the temperature and film thickness dependence of the flexoelectric coefficients. Recently, Stengel [18] built up a new continuum thermodynamic functional and constructed the relationship between the continuum description and *ab initio* phono dispertion curves, which was used to calculated the flexoelectric coefficients.

Besides of calculating the exact values of the flexoelectric coefficients, the upper limits for the magnitude of the static bulk flexoelectric coefficients in ferroelectrics

were determined by Yudin et al. [19]. By studying the requirement of stability of the parent phase, the upper bounds for the flexoelectric coefficients were derived as

$$f_{44}^2 < c_{44} g_{44} \tag{34a}$$

$$(f_{11} - f_{12})^2 < (C_{11} - C_{12})(g_{11} - g_{12}) \tag{34b}$$

2.4 Size Effect of Flexoelectric Response

The significance of the flexoelectric response is not only related to the magnitude of the flexoelectric coefficients but also to the strain gradients. The flexoelectric response is expected to be largely size-dependent and tends to be much stronger when the structural size scales down to nanometers because the strain gradients are closely linked with structural feature size. The size scale of strain gradients can be shown in a simple way as discussed by Majdoub et al. [20]. As shown in Fig. 3, consider two triangular inclusions with different length scales but the same aspect ratio, when they were subjected to the same stress, the strain distributions of the two inclusions would be identical. So the strain gradients scaled inversely with a_i, which was the distance between two points inside the inclusion.

Majdoub et al. [20] also investigated the flexoelectric size effects of piezoelectric and non-piezoelectric cantilevers by using both the flexoelectric continuum theory and the atomistic simulations. As illustrated in Fig. 4, when the thickness of the cantilever was below 10 nm, an apparent piezoelectric response can be found in non-piezoelectric paraelectric BTO which was attributed to the flexoelectricity. With the decrease of thickness of the cantilever, the piezoelectric response of paraelectric BTO became much stronger, and its piezoelectric constant could be as high as five times of the piezoelectric BTO constant when the thickness of the cantilever was

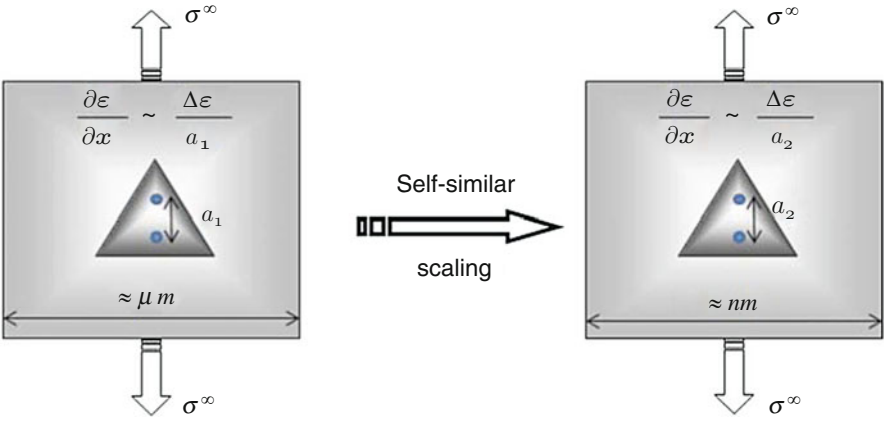

Fig. 3 The illustration of size effects of flexoelectricity by considering two triangular inclusions with the same aspect ratio, subjected to the same stress but with different length scales. Reprinted with permission from [20]. Copyright (2008) American Physical Society

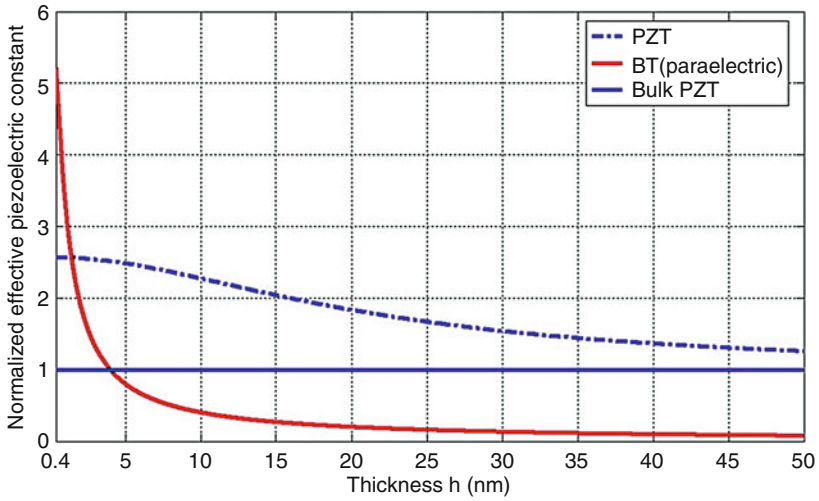

Fig. 4 The enhancement of piezoelectric response of piezoelectric PZT (*dashed blue*) and paraelectric BTO (*solid red*) with the decrease of cantilever thickness. The piezoelectric constants are normalized with respect to the bulk piezoelectric PZT (*solid blue*) ($d_{PZT} = -274pC/N$) and piezoelectric BTO ($d_{BT} = -78pC/N$), respectively. Reprinted with permission from [20]. Copyright (2008) American Physical Society

smaller enough. The enhancement of piezoelectric response of PZT (lead zirconate titanate) was relatively moderate compared with that of BTO, but the piezoelectric constant was still doubled at 15 nm. Inspired by the size effect of flexoelectricity, Majdoub et al. [21] also found a size-dependent effect of the harvested power of a PZT cantilever due to flexoelectricity. Their results indicated that the energy harvesting of piezoelectric nanostructures could be dramatically enhanced in a definite small range of sizes by taking the flexoelectricity into consideration.

Due to the size effects and its significance in smaller size, flexoelectric response is quite strong in systems with nanoscale sizes and comparable to the piezoelectric response or even plays a dominant role. To clarify the influence of flexoelectricity and its size effects in nanostructures, there are also more and more interests focused on the flexoelectric continuum theory, which will not be covered here, and are referred to, e.g., Reference [22].

3 Experimental Characterization of Flexoelectric Effect

3.1 Experimental Determination of Flexoelectric Coefficients

The measurement techniques of flexoelectric coefficients include direct methods and the converse ones. The direct methods measure the polarization of the samples induced by the external inhomogeneous deformations. In contrast, the converse methods utilize the converse flexoelectric effect, measure the strains of the sample under a nonuniform

electric field, and extract the converse flexoelectric coefficients. It has been shown that the direct and converse flexoelectric coefficients are equivalent. The direct methods are more commonly used and include various designs such as cantilever bending, three-point bending, four-point bending and pyramid compression, etc.

The typical experimental setups of cantilever bending, three-point bending, four-point bending and pyramid compression are illustrated in Fig. 5a, b, c and d, respectively. To illustrate the measurements, take the three-point bending measurement conducted by Zubko et al. [10] as an example. As shown in Fig. 5b, oscillatory bending strain can be induced by the probe on single crystal STO, with the strain gradient being

$$\frac{\partial \varepsilon_{11}}{\partial x_3} = 3z_0 \left(\frac{L}{2}\right)^{-3} \left(\frac{L}{2} - x_1\right), \tag{35}$$

where L is the distance between the knife edges under the sample, z_0 is the displacement of the probe, and x_i is the distance between the center of the sample and the interested position. The induced average out-of-plane polarization can be measured as

$$\overline{P_3} = \frac{I}{\omega A} \tag{36}$$

where ω is the angular frequency of the oscillatory mechanical bending, A is the area of the electrode and I is the measured ac current. In addition, the flexoelectricity-induced average polarization can also be obtained as

$$\overline{P_3} = \mu \overline{\frac{\partial \varepsilon_{11}}{\partial x_3}} = \mu \frac{12 z_0}{L^3} (L - a) \tag{37}$$

where μ is the effective flexoeletric coefficient and a is the half length of the electrodes. From Eqs. (36) and (37), it has

$$\mu = \frac{IL^3}{12\omega A z_0 (L - a)} \tag{38}$$

It should be noted that μ is the effective flexoelectric coefficient, which is a combination of the flexoelectric coefficients defined before. To obtain the full three flexoelectric coefficients of STO, the measurement should be repeated for samples with different orientations. It is also necessary to use a different method to get another independent equation because the pure bending method can only provide two independent equations. Then the flexoelectric coefficients can be extracted by solving the independent equations of different μ from different measurements. Moreover, the existence of the heater and liquid N_2 bath in Fig. 5b enables the controllability of temperature; thus, the dependence of the flexoelectric coefficients can also be obtained.

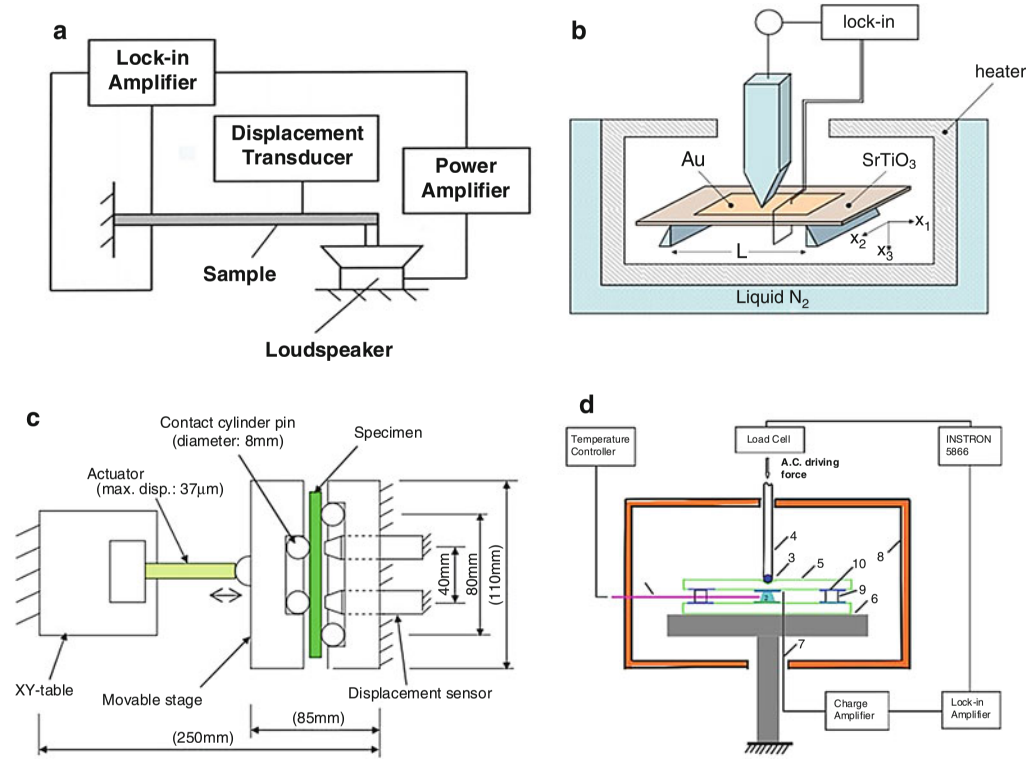

Fig. 5 The experimental setups for different direct measurement methods of flexoelectric coefficients. (**a**) Cantilever bending (Reprinted with permission from [9]. Copyright (2001) AIP Publishing LLC.), (**b**) three-point bending (Reprinted with permission from [10]. Copyright (2007) American Physical Society.), (**c**) four-point bending (Reprinted from [23]. Copyright (2011) The Japan Society of Mechanical Engineers.) and (**d**) pyramid compression. (Reprinted with permission from [24]. Copyright (2006) Springer Nature.)

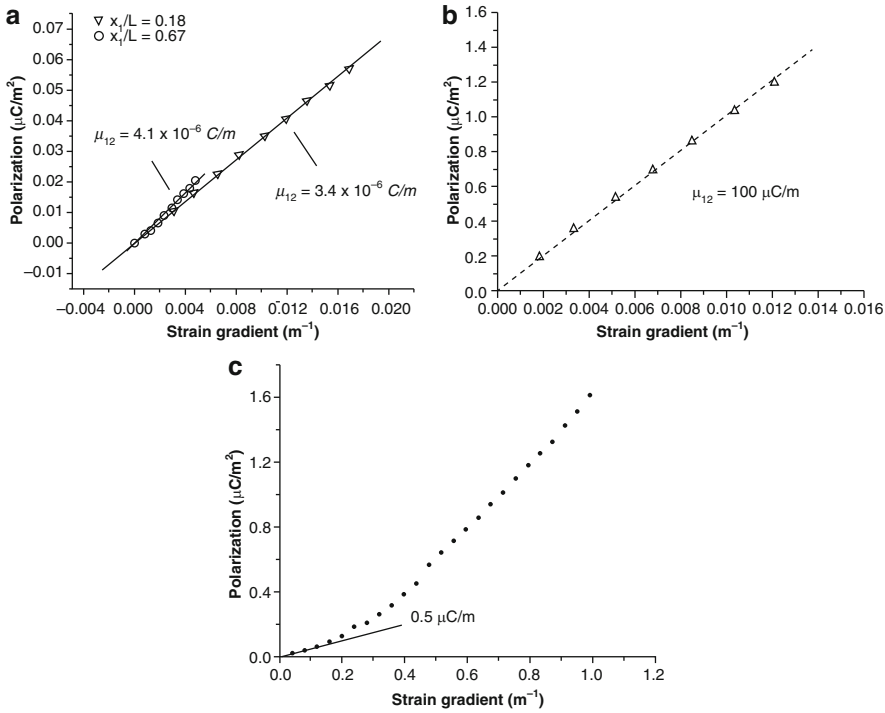

Fig. 6 The relationship between the flexoelectricity-induced polarization and strain gradient in (**a**) relaxor PMN (Reprinted with permission from [9]. Copyright (2001) AIP Publishing LLC.), (**b**) paraelectric BST (Reprinted with permission from [25]. Copyright (2002) AIP Publishing LLC.) and (**c**) unpoled ferroelectric PZT (Reprinted with permission from [26]. Copyright (2003) AIP Publishing LLC.)

By using the developed experimental techniques, the flexoelectric coefficients of a number of ferroelectric and relaxor ceramics have been measured. The results of the direct and converse methods show a good agreement. The relationships between the flexoelectricity-induced polarization and strain gradient of relaxor PMN (lead magnesium niobate), paraelectric BST (barium strontium titanate), and unpoled ferroelectric PZT are shown in Fig. 6. It can be seen that for paraelectric ceramics, the flexoelectric polarization scales linearly with strain gradient as expected. In contrast, for unpoled ferroelectric one, the flexoelectric behavior is nonlinear, which is associated with the ferroelastic domain switching under large mechanical loading.

According to Tagantsev [7], the relationship between flexoelectric coefficients and dielectric permittivity can be described as

$$\mu_{ij} = \gamma \chi_{ij} \frac{e}{a} \tag{39}$$

where χ_{ij} is the dielectric susceptibility and γ is a constant of the value close to 1.

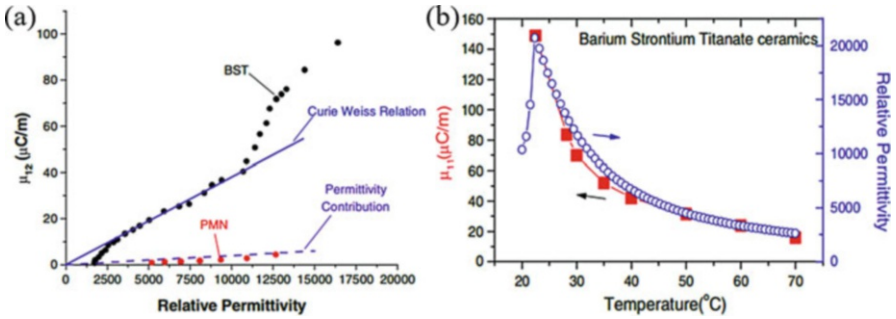

Fig. 7 (**a**) Relationship between flexoelectric coefficient μ_{12} and dielectric permittivity and (**b**) the temperature dependence of μ_{11} and χ of BST. Reprinted with permission from [24]. Copyright (2006) Springer Nature

The experimental results characterizing the permittivity dependence of μ_{12} for PMN and BST are shown in Fig. 7a. The temperature dependence of μ_{11} and χ of BST are shown in Fig. 7b. It is clear that the flexoelectric coefficients scale with the dielectric permittivity. The enhancement of μ_{12} in BST above ϵ_r~11000 is perhaps associated with the existence of ferroelectric domains above the general transition temperature. However, it can be seen that γ of PMN and BST are not as expected and are also much different with each other, with γ_{PMN}~0.65 and γ_{BST}~9.3. Moreover, for unpoled PZT and BTO ceramics, the scale factors have been determined as γ_{PZT}~0.57 and γ_{BT}~11.4, respectively. Compared with Pb-based PZT and PMN, the Ba-based BST and BTO have stronger flexoelectric effects and larger values of γ. Thus the chemical makeup might be the source of the difference of the flexoelectricity in these two perovskite structures.

The dielectric permittivity dependence of the flexoelectric coefficients indicate a large flexoelectric response at the temperature close to the paraelectric-ferroelectric transition temperature of ferroelectrics, where the ϵ_r is much higher. The measured flexoelectric coefficients of BST, PMNT (lead magnesium niobate-lead titanate), and PST (lead strontium titanate) under such conditions are indeed particularly high ($\sim 10 - 100\mu C/m$). But for relaxor ferroelectric PMN, the large μ_{12} is attributed to not only the large permittivity but also the reorientation of the polar nanodomains under strain gradients.

The flexoelectric coefficients have also been measured for some kinds of single crystals. The temperature dependence of the flexoelectric response of STO and BTO are shown in Fig. 8a and b, respectively. The inset of Fig. 8a shows the linear proportionality between flexoelectricity-induced polarization and strain gradients, as expected. For STO, the flexoelectric response increases qualitatively following the dielectric permittivity with a decreasing temperature. However, there is an anomaly of the flexoelectric response when the temperature is below 105K, which is the cubic to tetragonal phase transition temperature of STO. The anomaly can be explained as follows: ferroelastic domains appear below 105K and tend to release the elastic energy by readjustment of domain walls under mechanical deformation, thus leading

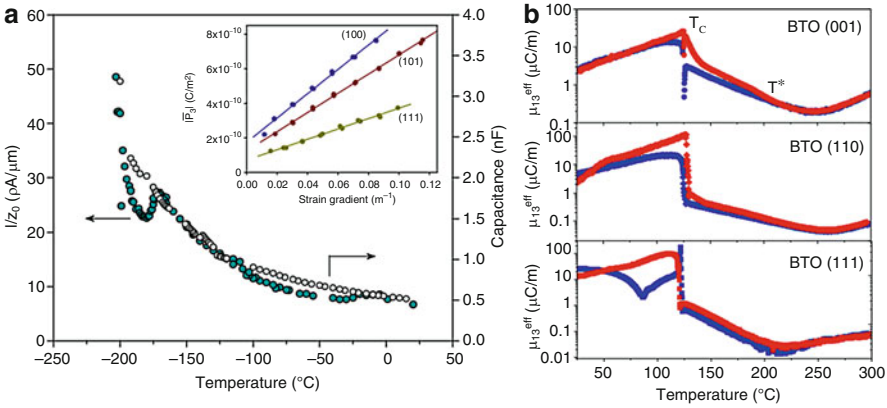

Fig. 8 Temperature dependence of the flexoelectric response of (**a**) single crystal STO (Reprinted with permission from [10]. Copyright (2007) American Physical Society.) and (**b**) single crystal BTO. The inset of a shows the relationship between the polarization induced by flexoelectric effect and strain gradient. The red and blue curves in b are the measured values on heating and cooling, respectively (Reprinted with permission from [27]. Copyright (2015) American Physical Society.)

Table 1 Flexoelectric coefficients for BTO and STO from theoretical calculations and experiment. Reprinted with permission from [13]. Copyright (2009) American Physical Society.

	$\mu_{11}(10^{-13}$C/m)		$\mu_{12}(10^{-13}$C/m)		$\mu_{44}(10^{-13}$C/m)	
	Ab initio	Experiment	Ab initio	Experiment	Ab initio	Experiment
STO	−26.4	20	−374.7	700	−357.9	300
BTO	15.0		−546.3	10^6	−190.4	

to the relaxation of strain gradients and consequently the reduction of the flexoelectric response. For BTO single crystal, a sharp decrease of flexoelectric coefficients from 10–100 μC/m to 1–10 μC/m can be seen above T_c, which corresponds to the ferroelectric-paraelectric phase transition. Since the reported values of BTO ceramics in paraelectric phase are 5–50 μC/m, it indicates that the grain boundaries play a role of enhancing the flexoelectric response.

To compare the flexoelectric coefficients obtained through theoretical calculations and experimental measurements, BTO and STO are taken as examples as displayed in Table 1. It can be seen that the order of magnitude of flexoelectric constants for STO show good agreement between the ab initio calculations and the experiments, while the measured transverse flexoelectric coefficient of BTO are three to four orders higher than the calculated one. This discrepancy is partly attributed to the large temperature dependence of the dielectric permittivity of BTO, since the temperature of the calculation is 0K, while the experiment is conducted at room temperature. Taking this effect into consideration, the gap can be narrowed to about one to two orders of magnitude. Other sources of this gap involve the surface piezoelectricity and the flexoelectricity-induced alignment of

precursor polarization existing in the paraelectric phase of BTO. Furthermore, since the experimental data for BTO used here is from BTO ceramics, the grain boundary enhancement of flexoelectricity is also a contribution to this gap.

4 Flexoelectricity-Induced Novel Phenomena in Nano-ferroelectrics

When the size of ferroelectric system decreases to nanoscale, various triggering phenomena arise. Many of the phenomena can be explained without taking into account the flexoelectric effect, while some of the anomalies cannot. In this section, we will discuss the triggering phenomena and properties induced by flexoelectric effect in nanoscale ferroelectrics, from relatively global characteristics such as dielectric responses and imprint behaviors to some local characteristics, e.g., the profile and conductivity of domain walls.

4.1 Modifications on Dielectric and Mechanical Response of Nanoscale Ferroelectrics

4.1.1 Modified Dielectric Response

It has been reported that for ferroelectric thin films close to the transition temperature, the permittivity is depressed rather than the sharp peak of bulk ferroelectrics. With decreasing film thicknesses, the depression tends to be more pronounced. The smearing of the temperature-dependent permittivity for BST thin films with different thicknesses is shown in Fig. 9a. By taking the flexoelectric effect into consideration, Catalan et al. [29] calculated the ferroelectric properties in terms of the LGD theory in the assumption of an exponentially relaxed strain profile. The results show a good agreement with the experimental data, as displayed in Fig. 9b. Unlike bulk ferroelectrics, thin films are subjected to misfit strains by the underlying substrates. The misfit strains relax across the direction of film thickness and generate a strain gradient in the film. Due to the flexoelectric effect, this strain gradient will induce a built-in flexoelectric field, which influence the dielectric responses. With decreasing film thickness, the flexoelectric response becomes more apparent and leads to a larger degradation of the dielectric permittivity.

Besides the smearing of the dielectric permittivity, flexoelectricity can also modify the critical thickness of the ferroelectric films. The reported vanishing critical thickness of free standing PT (lead titanate) films has been demonstrated to be caused by flexoelectricity. And it is proposed that the critical thickness of epitaxial BTO films can be increased by the flexoelectric effect. Furthermore, the flexoelectricity-induced modifications on Curie temperature and pyroelectric coefficients of ferroelectric thin films have also been reported. These phenomena indicate that thin films with desirable dielectric and ferroelectric properties could be designed by introducing or avoiding specific strain gradients.

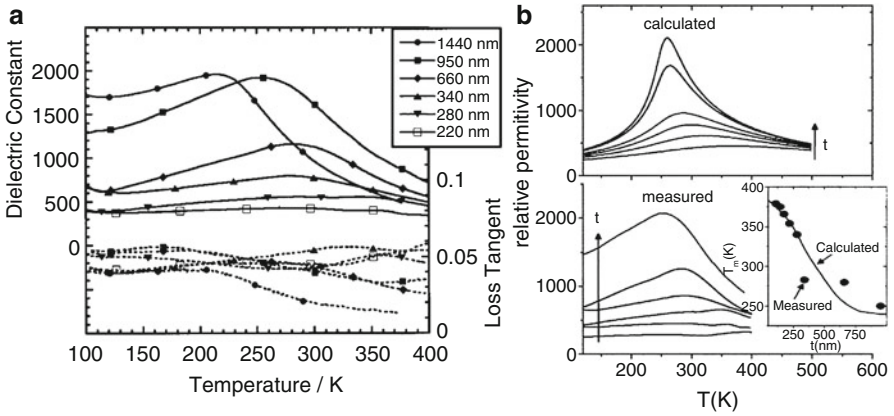

Fig. 9 (**a**) Experimental data of relative permittivity for BST grown on SRO substrate (Reprinted with permission from [28]. Copyright (2002) AIP Publishing LLC.) and (**b**) The calculated temperature dependence of permittivity and the comparison with the measured values (Reprinted with permission from [29]. Copyright (2005) American Physical Society.)

4.1.2 Modified Mechanical Response

In indentation tests of ferroelectrics, it is found that the indentation hardness was enhanced when the indenter radius decreases. This indentation size effect of hardness is demonstrated to be induced by the flexoelectric effect by Gharbi et al. [30], both theoretically and experimentally. Barium titanate and quartz were both investigated to testify their theory. The indentation hardness with different indenter radius is shown in Fig. 10a. It can be seen that the flexoelectric model is in excellent agreement with experiments. For macroscale indentation, the strain field is relatively uniform, and the strain gradient is small; therefore, the flexoelectricity-induced enhancement can be neglected. For nanoscale indentation, there existed an extremely large strain gradient so that the enhancement is apparent for BTO which has large flexoelectric coefficients. While quarts shows no enhancement even for nanoindentation because of its weakness of flexoelectric response. This enhancement phenomenon also provides us a method to extract the flexoelectric coefficients by indentations. For BTO in the present case, the extracted flexoelectric coefficients is $\mu_{12} = 4\mu$C/m, which is in good agreement with the value measured by cantilever bending.

In fact, besides the indentation hardness, various mechanical properties are modified by flexoelectricity and thus present a size effect according to the developed flexoelectric continuum theory. As an example, the effective flexural stiffness of PMN nanofilm is shown in Fig. 10b. It can be seen that correction of flexural stiffness due to flexoelectricity is fairly obvious when the film thickness decreases to several nanometers and cannot be neglected in the design and fabrication of nanodevices.

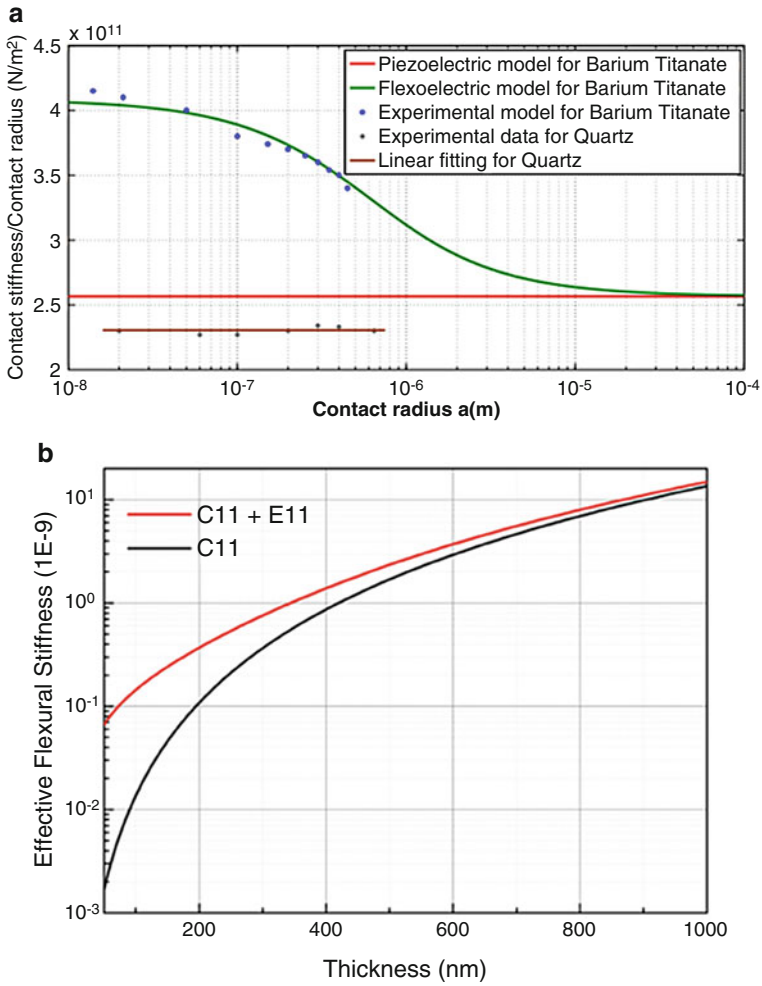

Fig. 10 (**a**) Size effect of the indentation hardness of BTO and quartz (Reprinted with permission from [30]. Copyright (2009) AIP Publishing LLC.). (**b**) Effective flexural stiffness of PMN nanofilms. The *red line* is based on the flexoelectric theory, and the *blue curve* represents the classical piezoelectric theory (Reproduced from [31]. © IOP Publishing Ltd. All rights reserved.)

4.2 Imprint Behaviors in Ferroelectric Nanofilms

The phenomenon that the polarization of ferroelectrics has a preferential direction and asymmetric hysteresis loops is known as imprint. That is, one polarization state is more stable than the other. This asymmetric polarization bistability on the one hand will degrade the performance of devices such as nonvolatile memory in ferroelectric thin film; on the other hand, it can also lead to an interesting

phenomenon, such as smearing of phase transition. Ferroelectric nanocapacitors are typical examples to exhibit imprint behavior. For these systems, first-principle calculations have showed that the different bonding environment at the top and bottom electrode/ferroelectric interfaces can lead to asymmetric stability of polarization. (See reference [32] and references therein.) Meanwhile, phenomenological models usually attribute the intrinsic source of this asymmetric polarization stability to the so-called non-switchable dead layer at the film/electrode interface. This layer may be caused by various reasons such as a secondary low-permittivity phase at the film surface, the presence of misfit dislocations, nearby-surface variation of polarization and electric field penetration into the electrodes, etc.

Importantly, it has been demonstrated that the dominant contribution to the dead layer is the flexoelectric effect trigged by the large strain gradient near the interface. The misfit strain between the film and electrode relaxes by the appearance of dislocations. Full strain relaxation will generate a strain gradient as large as $\sim 10^6$ m^{-1} with a relaxation length of 10 nm. The flexoelectric filed is estimated as $E_f = f \nabla\varepsilon \sim 10^7$ V/m by using the typical value of the flexocoupling coefficients $f \sim 10$ V. Although this estimated value is smaller than value of the coercive field, it is thought to result in the non-switchable dead layer at the region of interface, as shown in Fig. 11. Assuming the direction of flexoelectricity-induced polarization in the dead layer is upward, as illustrated, the head-to-head polarization configuration of the capacitor will result in a larger electrostatic energy compared with the head-to-tail configuration and is less energetically favorable. This leads to a preferential polarization oriented upward in the rest of the film; thus, imprint behavior occurs. This flexoelectricity-induced imprint behavior reminds us that large strain gradients need to be avoided to prevent the degradation of device performance in ferroelectric nanofilms.

Imprint behavior can also be introduced by the application of external strain gradients. Gruverman et al. [34] demonstrated that the PZT thin films could be imprinted through flexoelectric effect by applying bending stress. The PFM

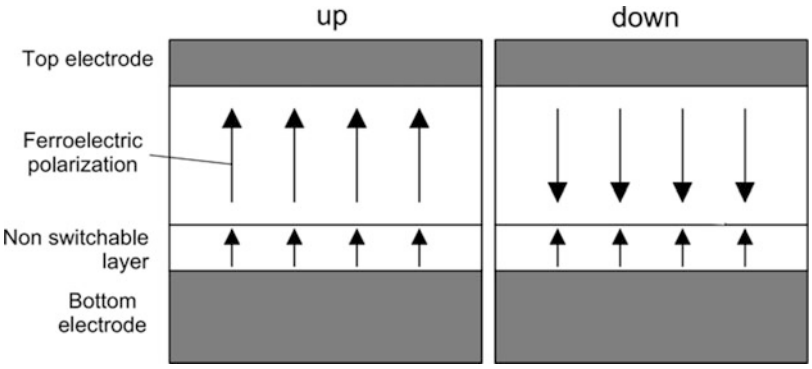

Fig. 11 Schematics of non-switchable dead layer at the region of interface of a ferroelectric capacitor. Reprinted with permission from [33]. Copyright (2006) AIP Publishing LLC

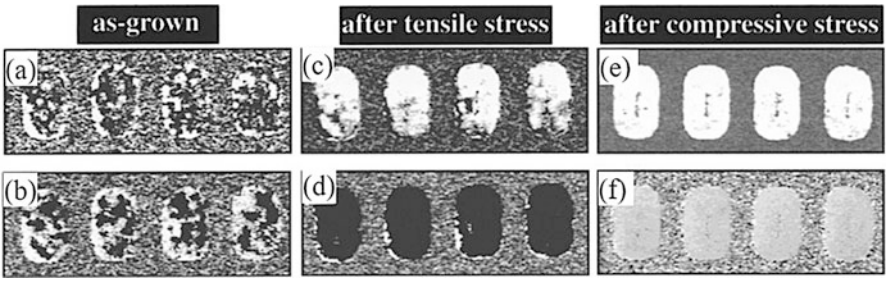

Fig. 12 Imprint behavior generated by mechanical bending in PZT thin film. (**a**) and (**b**) are the PFM amplitude and phase images for the as-grown film before bending. (**c**, **d**) and (**e**, **f**) are the corresponding images after tensile and compressive bending, respectively. Reprinted with permission from [34]. Copyright (2003) AIP Publishing LLC

magnitude and phase images of the as-grown film are shown in Fig. 12a and b. Corresponding images after tensile and compressive bending are shown in Fig. 12c, d, e and f, respectively. The dark and light regions in phase images represent the upward and downward polarization, respectively. The dark lines in the amplitude image represent the domain boundaries. It can be seen that before bending, the polarization has no preferential direction. After the application of tensile bending stress, the as-grown capacitor is switched into a single domain with upward polarization, while the application of compressive bending stress results in a single domain with downward polarization. The different preferential polarization directions are due to the opposite sign of the strain gradient for tensile and compressive bending. This kind of imprint behavior suggests that the domain configurations of nano-ferroelectrics can be influenced and controlled by external strain gradients, which will be discussed in detail in the next section.

4.3 Influence of Flexoelectric Effect on Ferroelectric Nanodomains

4.3.1 Mechanical Switching of Polarization in Ferroelectric Thin Films

Since the flexoelectric field induced by strain gradients is analogous to electric field, it can also be used to switch the polarization of ferroelectrics mechanically. The experimental demonstration of the mechanically induced domain switching was conducted by Lu et al. [35]. BTO ultrathin film grown on STO substrate was used in their investigation. The compressive misfit strain of the film resulted in the out-of-plane polarization; thus, only 180° polarization switching was allowed. The film was first written into a bipolar domain state electrically, the PFM images of which are shown in Fig. 13a and b. Then it was scanned in the center area by an AFM tip with an increasing loading force from 150 to 1500 nN. The PFM images of the scanned film are shown in Fig. 13c and d. It can be seen that with increasing tip force, the upward polarization is switched downward. This mechanical switching behavior is

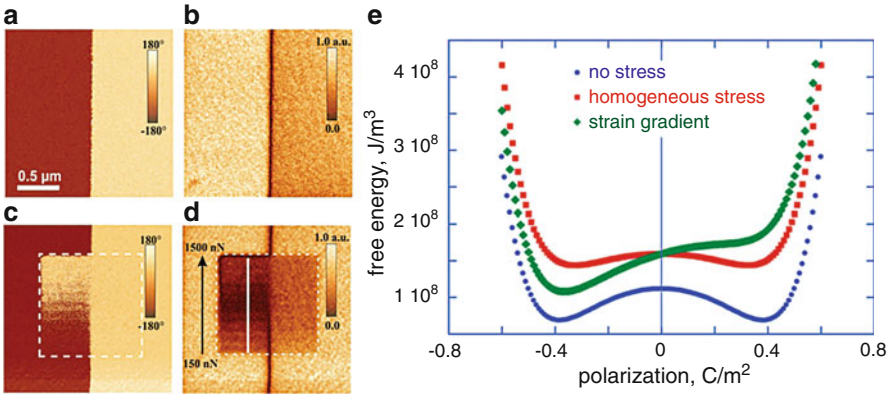

Fig. 13 Mechanically induced reversal of ferroelectric polarization. (**a**) and (**b**) are the PFM phase and amplitude images of the film in bipolar states. *Dark areas* in the phase image represent the domain with upward polarization. (**c**) and (**d**) are the PFM phase and amplitude images after scan. (**e**) Free energy calculations for the epitaxially clamped BTO ultrathin film subjected to no stress (*blue curve*), homogeneous compressive (*red curve*), and tip-induced strain gradient (*green curve*). From [35]. Reprinted with permission from AAAS

attributed to the flexoelectric filed induced by the local stress inhomogeneity under the AFM tip. The estimated flexoelectric field is as strong as 2 MV/cm, which is comparable to the coercive field. This switching behavior can also be explained in perspective of free energy. Figure 13e shows the calculated free energy for the epitaxially clamped BTO ultrathin film under no stress, homogeneous compressive stress, and tip-induced strain gradient. Under homogeneous stress, the double well is still symmetric though the barrier decreased. While under strain gradient, the double well is skewed, and the downward polarization state is more energetically favorable, thus driving the upward polarization to switch downward.

The effects of epitaxial strain on mechanical switching were investigated, and it was found that the mechanical threshold for polarization switching increased with increasing in-plane compressive strain, which was resulted from the increase of coercivity and tetragonality. The loading mode of AFM tip was also reported to influence mechanical switching process and resulting domain. Sliding contact loading mode requires smaller load to realize the switching, and the written domains were much more stable, compared with the perpendicular loading mode. This was attributed to the different strain distributions under the AFM tip in different loading modes. The nonvolatile ferroelectric memory written mechanically and read electrically were recently demonstrated in ferroelectric polymer. The force needed to record electronic signals on the polymer film was less than 100 nN and the mechanically written domains were stable and electrical erasable.

Note that the flexoelectric field induced by the AFM tip is localized near the tip, which makes it suitable to write local nanodomains but not suitable to erase them. From theoretical point of view, a nonlocal flexoelectric field can be also induced by other kinds of strain gradients such as when a nanofilm is subjected to cylindrical

bending or wavy bending. Simulation has showed that the nonlocal flexoelectric fields associated with these two kinds of mechanical bending can largely affect the stability of the nanodomains in ferroelectric nanofilm and lead to effective erasing of the information stored by the nanodomains [36]. Take the wavy bending as an example, as illustrated in Fig. 14.

To study the erasing effect of wavy bending, the stability of pre-written 180° cylindrical domains with different sizes are investigated. The strain profile of a nanofilm under wavy bending can be approximately descriped as a cosine form (Fig. 14a). The flexoelectric effect is considered with a flexocoupling $f_{12} = 10V$. Fig. 14b and c depict the distributions of in-plane strain and the flexoelectric field and as a function of the wave amplitude. Firstly, it can be seen that wavy bending has significant impact on the stability of cylindrical domains, which can lead to the instability of domains and thus lead to the erasing effect. As shown in Figure. 14d, where the flexoelectric field is switched off, the critical size of stable cylindrical domain changes from 11 nm to 30 nm when the bending amplitude increases from 0.2 nm to 1.0 nm. When the flexoelectric field is switched on, significant difference can be found in the controllability on domain stability of the bending loads (Fig. 14e). Flexoelectric field can both enhance and depress the stability of the 180° cylindrical domain, depending on the direction of the domain polarization and the flexoelectric field. Due to the modulated flexoelectric field, large change in domain shape not only happens at region near domain instability but also happens when the domain size is comparable to the wave length, as indicated by the $<P_3>$ curves as shown in Fig. 14g. By influencing the stability of domains, the nonlocal wavy bending and flexoelectricity can be used to erase information, and furthermore, control the domain shapes.

Compared with electrical switching, mechanical switching can avoid the associated breakdown and leakage problem. As the critical mechanical load to induce polarization switching is generally small, the nanofilm cannot be damaged in the mechanical switching process. It is therefore promising for application in nonvolatile ferroelectric memory with ultrahigh data storage density and less power consumption. However, mechanical switching has only been reported to switch the upward polarization to downward, not vice versa. The reversal switching may be realized by strain gradient engineering or by changing the surface screening condition of the film, which so far has not yet been investigated.

4.3.2 Impacts on Domain Patterns of Nanoscale Ferroelectrics

The properties of ferroelectrics such as dielectric and piezoelectric response can be largely modified by the domain structure. Since flexoelectricity is significant at nanoscale, its effect on the domain configurations should be considered for applications of ferroelectrics. The influence of flexoelectricity on the domain patterns of $HoMnO_3$ epitaxial thin films has been reported by Lee et al. [37]. To investigate the role flexoelectricity, films with different large strain gradients were grown. The strain gradients were modulated by controlling the oxygen partial pressures P_{O2} during the growth process. Figure 15a shows the strains for films deposited at high and low P_{O2}. It can be seen that strains for both high and low P_{O2} were relaxed exponentially from the film/substrate interface to the film surface, and the strain variation for high P_{O2} is

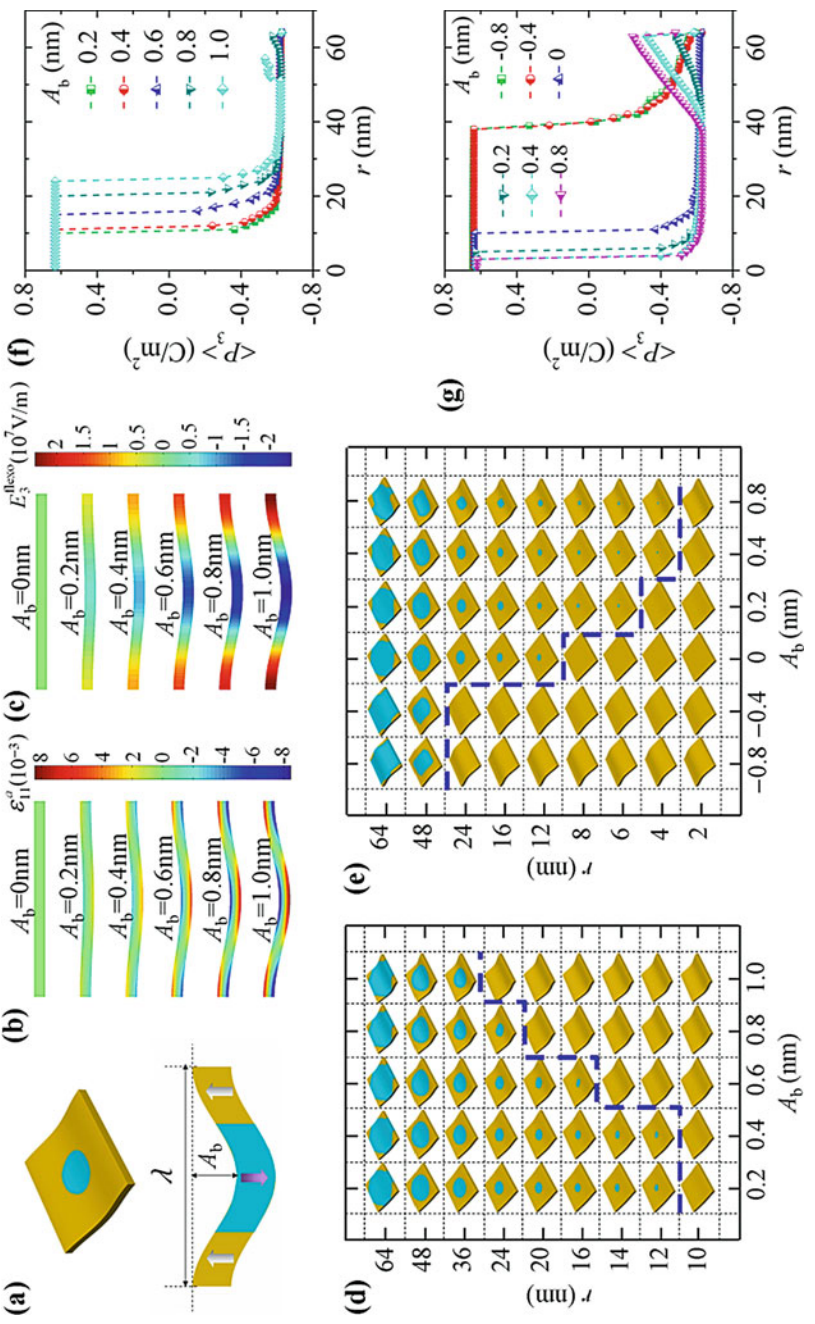

Fig. 14 (continued)

larger than low P_{O2}. Thus the films deposited at higher P_{O2} had larger strain gradient. It was estimated that the flexoelectric field E_s for film grown with $P_{O2} = 10$ mTorr and $P_{O2} = 350$ mTorr was ~0.7MV/m and ~5MV/m, respectively. The estimated values of E_s were comparable to the coercive filed of the film at temperature close to T_c so the flexoelectric effect was giant. The domain configurations for films deposited at different P_{O2} are shown in Fig. 15b. For the film deposited at low P_{O2} with small E_s, a mixed multidomain pattern was formed due to the depolarization energy. Meanwhile, for the film deposited at high P_{O2} near T_c, E_s was large enough to induce the formation of monodomain. The effect of E_s on the domain configurations was further investigated by a periodic two-dimensional model illustrated in Fig. 15c, where α and β are the domain width of the upward and downward domains. The results are shown in Fig. 15d. It can be clearly seen that the flexoelectric field had a large effect on the domain configurations, which indicated that the domain configurations could be tuned by flexoelectricity.

Another experimental evidence suggesting that the flexoelectricity had effect on the domain configurations was reported by Catalan et al. [38]. They noticed that there existed large unexpected horizontal strain gradients in the *c*-domains of PTO thin film with *a*-*c* twins. The strain gradients were attributed to the attachment of the film with ferroelastic domains onto the flat surface of the substrate. According to flexoelectricity, this strain gradient would lead to a horizontal contribution to the polarization of *c*-domain and cause a strong polarization rotation. They measured the lattice distortion (Fig. 16a) and mapped polarization of the twins in the film (Fig. 16b). Strong polarization rotation of *c*-domains was observed, which was in agreement with the flexoelectric theory.

The influence of flexoelectricity on domain configurations was also theoretically investigated by Ahluwalia et al. [39]. They predicted the domain patterns under different strength of the flexoelectric coupling by using two-dimensional phase field simulations. The roles of different flexoelectric components were also analyzed under mechanically constrained and stress-free boundary conditions. It was found that a fine structure in domain patterns formed when the strength of flexoelectric coupling exceeded a critical value, as shown in Fig. 17a. The polarization (P_y in Fig. 17b) in these fine domains had a nearly sinusoidal modulation, indicating the formation of the so-called "incommensurate" or modulated phase. The finding that flexoelectricity could induce incommensurate phase formation in ferroelectrics was in agreement with previous investigations. Two-dimensional modulated domain

Fig. 14 Control of domain stability by wavy bending on 128 nm × 128 nm × 8 nm simulation cells at room temperature. The cells are initially written with cylindrical domains with size r from 1 nm to 64 nm. (**a**) Schematics of a cell under wavy bending, with $\lambda = 128$ nm. Distributions of (**b**) strain and (**c**) flexoelectric field as a function of A_b in the x-z plane of a cell under wavy bending. Phase diagrams of equilibrium domain pattern in cells under wavy bending with flexoelectric field (**d**) switched off and (**e**) on. (**f**) and (**g**) the average polarization of the equilibrium domain patterns in z-direction, i.e., $<P_3>$, in the initial cylindrical domain region, for the two bending cases. Reprinted with permission from Macmillan Publishers Ltd. Nature Scientific Reports [36], Copyright (2014)

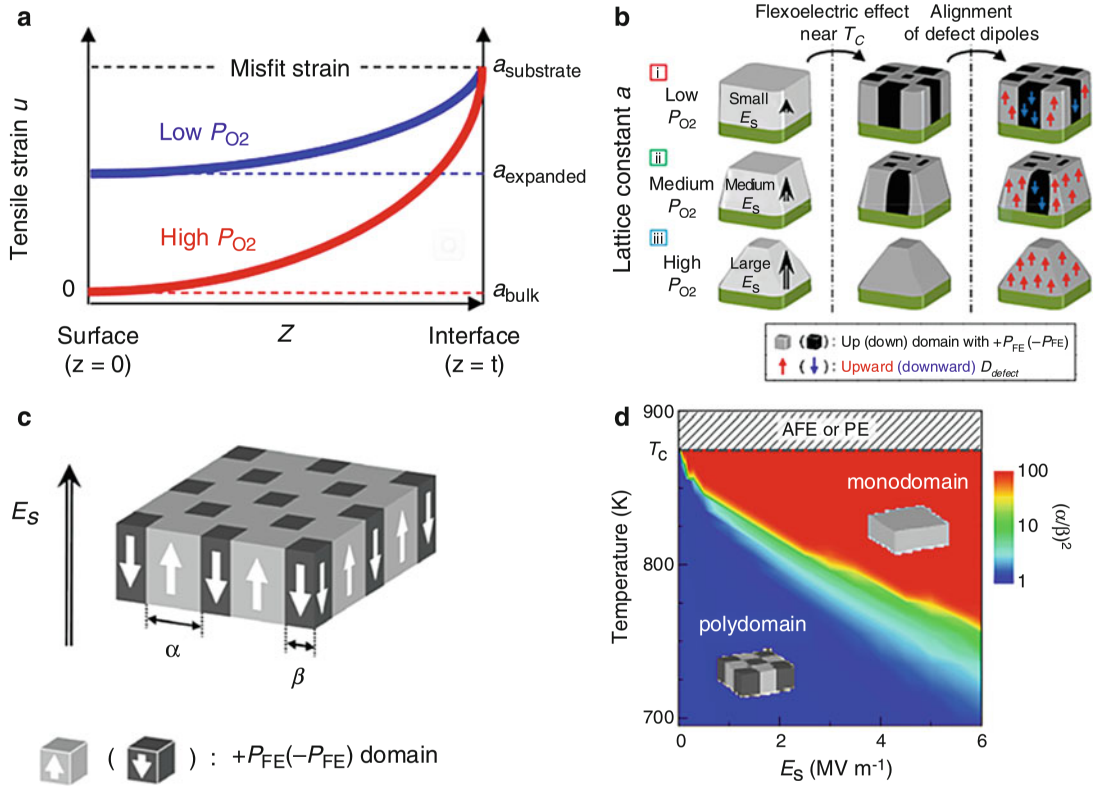

Fig. 15 Flexoelectricity tuned domain configurations. (**a**) Strain profiles for films deposited at high and low P_{O2}. (**b**) Schematic diagram showing how E_s can affect domain configuration, which depends on P_{O2} during the growth process. (**c**) A simple model of two-dimensional periodic square-like 180° domains. (**d**) Temperature and E_s dependence of the domain configuration. Reprinted with permission from [37]. Copyright (2011) American Physical Society

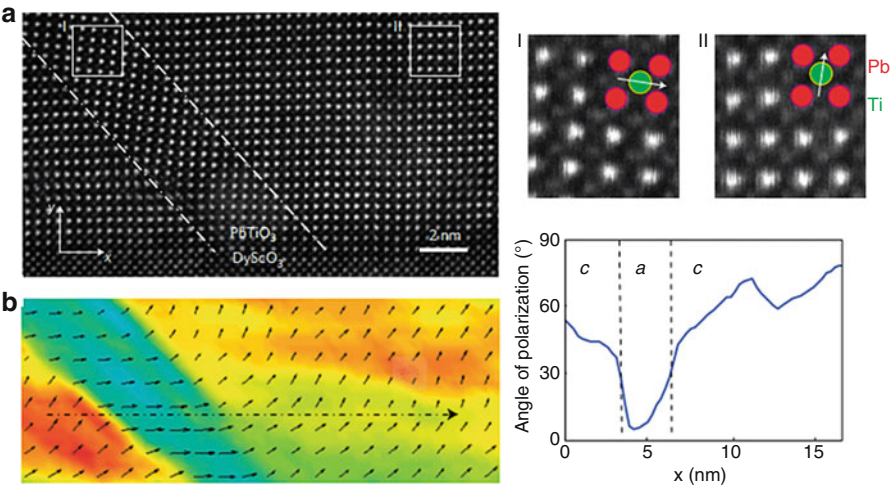

Fig. 16 Direct observations of the polarization rotation. (**a**) Positions of atoms with zoom-ins showing the *a*-domain (I) and *c*-domain (II). (**b**) Out-of-plane strain (*color map*) and electric polarization (*vector map*) with the line scan showing the rotations angles from normal in the *c*-domains. Reprinted with permission from Macmillan Publishers Ltd. Nature Materials [38], Copyright (2011)

patterns, such as domain patterns with alternating vortices (Fig. 17c) and with coexisting phases of the stripes and vortices (Fig. 17d), had also been observed under specific flexoelectric coupling strengths and mechanical boundary conditions. It was proposed by the authors that more flexoelectricity-induced domain configurations might occur in the real 3D crystals. It is noteworthy that effect of mechanical strain/stress on the vortex transformation has been revealed [40], which showed quite distinct characteristics from that of conventional electric field. Considering the similarity between flexoelectric field and electric field, mechanical strain/stress gradients might act like the role of electric field to induce transformation of ferroelectric vortices. However, it is still not clear now.

Furthermore, the controllability of domain evolution by mechanical loads and flexoelectricity has been reported by Chen et al. [41]. They investigated the stability and evolution paths of domain patterns under uniform strain and cylindrical bending strain gradient in ferroelectric nanofilms. The role of both the bulk and surface contributions to the flexoelectricity was studied for different initial domain patterns.

According to their results, the domain patterns were largely affected by strain gradient even in the absence of flexoelectricity. The presence of bulk flexoelectricity made the *a/c* and *b/c* domain variants more favorable and thus modified the domain patterns. Due to the weakness of the bulk flexoelectricity, this modification is small. The contributions of bulk flexoelectricity to the mechanical and polarization boundary conditions also had effects on the domain patterns. The domain pattern evolution was further investigated with different strength of flexoelectric fields, which involves both the bulk and surface contributions of flexoelectric effect. It was demonstrated

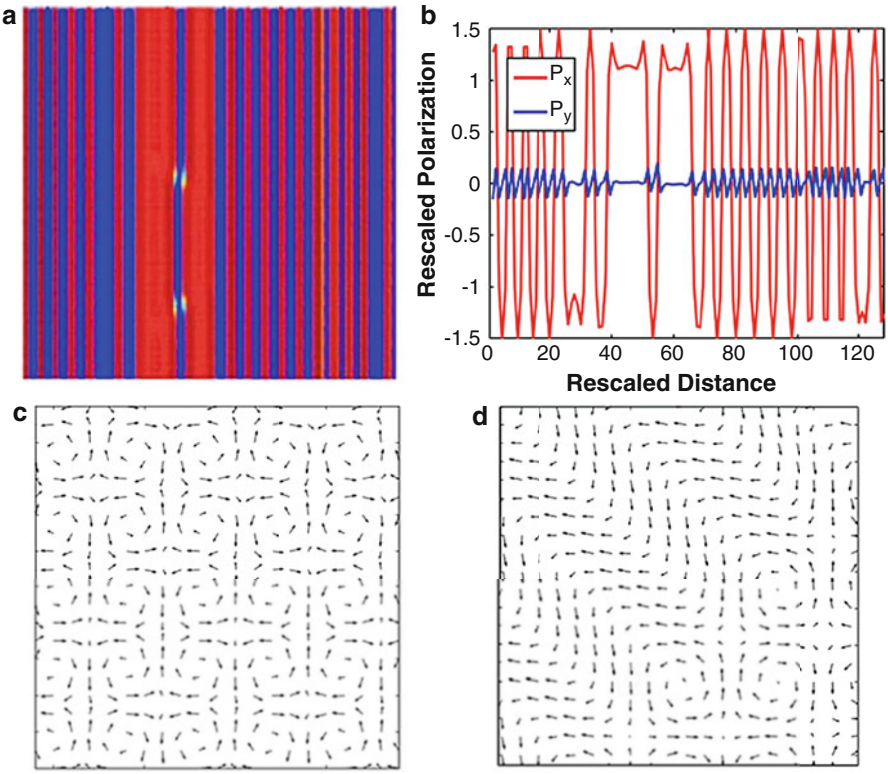

Fig. 17 (**a**) Domain pattern with $f_{44} = 15$ V under stress-free boundary conditions. (**b**) Polarization profile of the domain pattern in **a** along the x direction. (**c**) Domain pattern with $f_{11} = 15$ V under stress-free boundary conditions. (**d**) Domain pattern with $f_{11} = 12$ V under mechanically constrained boundary conditions. Reprinted with permission from [39]. Copyright (2014) American Physical Society

that with large flexoelectric field, the domain patterns were switched into the monodomain state, which indicating the erasing effect. The domain evolution of a nanofilm written with "SYSU" under various bending loads was investigated to show the effect of mechanical loads on the carried information in the film, as shown in Fig. 18. One can see that with the combined effect of strain gradient and flexoelectric field, the information was erased under a large downward bending. While under upward bending, the written information would be unstable and evolved to a lager domain, which could be used to assist writing domains.

4.4 Novel Domain Wall Properties Resulted by Flexoelectric Effect

Compared with domains, domain walls have been demonstrated to own attracting properties such as high electronic conductivity, chirality, and oxygen vacancy

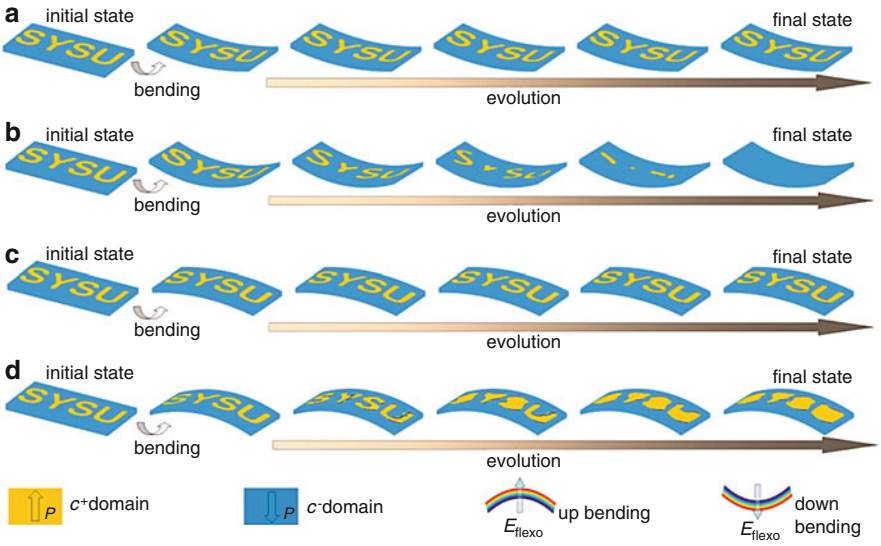

Fig. 18 Evolution of a written domain pattern "SYSU" under various cylindrical bending condition. (**a**) $\varepsilon_{top} = -\varepsilon_{top} = -0.005$, (**b**) $\varepsilon_{top} = -\varepsilon_{top} = -0.01$, (**c**) $\varepsilon_{top} = -\varepsilon_{top} = 0.005$, and (**d**) $\varepsilon_{top} = -\varepsilon_{top} = 0.01$. Reprinted from [41], Copyright (2015), with permission from Elsevier

segregation in ferroelectrics. It is becoming a trend to regard domain walls as promising alternative engineering elements in smart materials. Due to the sharp change of order parameter normal to the ferroelectric domain wall, the strain gradients in the wall can be very large as a result of electrostriction. Therefore the flexoelectric effect is very pronounced and has important effects on the domain wall properties.

4.4.1 Domain Wall Profile

The 180° domain wall separating domains with antiparallel polarizations is very common in ferroelectrics. The profile of this kind of domain wall has been considered as Ising-like for a long time. However, this viewpoint should be renewed by considering flexoelectric effect because the flexoelectricity-induced polarizations can result in more complicated domain wall profiles. The role of flexoelectricity on domain wall profiles has been reported recently. As an example, we discuss the domain walls of tetragonal BTO. Following the work of Gu et al. [42], consider a 180° domain wall with spontaneous polarization along x_3, as illustrated in Fig. 19a. The calculated domain wall by phase field simulation at wall orientation $\theta = 0$ is shown in Fig. 19b. Nonzero sinusoidal P_1 is observed, while P_2 is exactly zero, which corresponds to a Néel-like feature. Considering the dependence of flexoelectric and electrostrictive coefficients on domain wall orientation, the effect of flexoelectricity on domain wall profile is anisotropic. The calculated maximum absolute values of P_1 and P_2 in different oriented domain wall are shown in Fig. 19c.

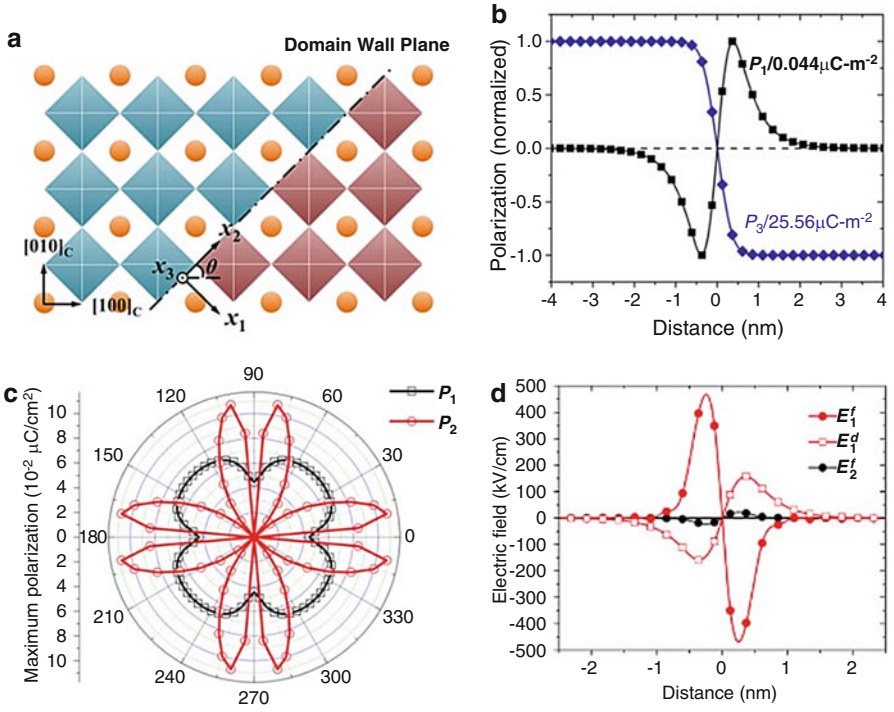

Fig. 19 (**a**) 180° ferroelectric domain walls in tetragonal BTO. x_1 is normal to the domain wall plane, while x_2 and x_3 are parallel to the domain wall plane. θ indicates the angle between domain wall and crystallographic direction $[100]_C$. (**b**) Domain wall profile of phase field simulation at $\theta = 0$. (**c**) Maximum absolute values of P_1 and P_2 vs. domain wall orientation θ. (**d**) Flexoelectric filed E_i^f and depolarization field E_i^d around the domain wall with $\theta = 5\pi/12$. Reprinted with permission from [42]. Copyright (2014) American Physical Society

As expected, a strong angular dependence of P_1 and P_2 is observed. The P_1 component is nonzero for all orientation θ, while P_2 vanishes when $\theta = n\pi/4$, with n being an integer, indicating that the pure ferroelectric domain wall is Ising-Neel type when $\theta = n\pi/4$ and Ising-Bloch-Neel type for all other orientations. In addition, since the strain resulted from the electrostrictive effect is symmetric with respect to the center of the domain wall, the flexoelectric filed proportional to strain gradient is along opposite direction on opposite side of the wall center, as shown in Fig. 18d, thus leading to the chiral profiles of P_1 and P_2 in tetragonal BTO domain walls. It should be noted that the chirality of P_1 induces a strong depolarization filed (see Fig. 19d), which would further influence the conductivity of the domain walls, as will be discuss later.

The flexoelectricity-induced non-Ising characteristics of domain wall profiles are in agreement with previous first-principle investigations, where the Bloch-like and Ising-like characters were reported but not explained. Furthermore, it should be noted that the polarization component normal to the domain walls (P_1 here) was also

found to be nonzero in other kinds of domain walls [43]. In incipient ferroelectrics STO, for example, polar ferroelastic twin walls have been predicted theoretically and confirmed experimentally. The polarization of its domain walls was attributed to flexoelectricity and rotostriction (or the so-called flexo-roto field), analogous to the mechanism in ferroelectrics, i.e., flexoelectricity and electrostriction.

4.4.2 Conductivity of Domain Walls

With different rotation angles with respect to the spontaneous polarization, ferroelectric domain walls can be nominally charged or not, as illustrated in Fig. 20a. Compared with the domain regions far from the domain walls, charged domain walls possess enhanced conductivity due to the accumulation of free charge carriers by screening the bound charges in the wall. Recently, the nominally uncharged ferroelectric domain walls and ferroelastic twin walls are also reported be conductive or with enhanced conductivity. It has been demonstrated that the conductivity of uncharged domain walls is closely related to flexoelectricity. Due to flexoelectricity, the polarization components and the domain wall profile are modified, as discussed in the previous section. The presence of polarization component perpendicular to the domain wall plane changes the bound charge distribution and results in a strong electric field at the wall. The accumulation of free screening charge carries is thus affected, and the modification on the domain wall conductivity arises. It should be noted that the domain wall conductivity was influenced by inhomogeneous

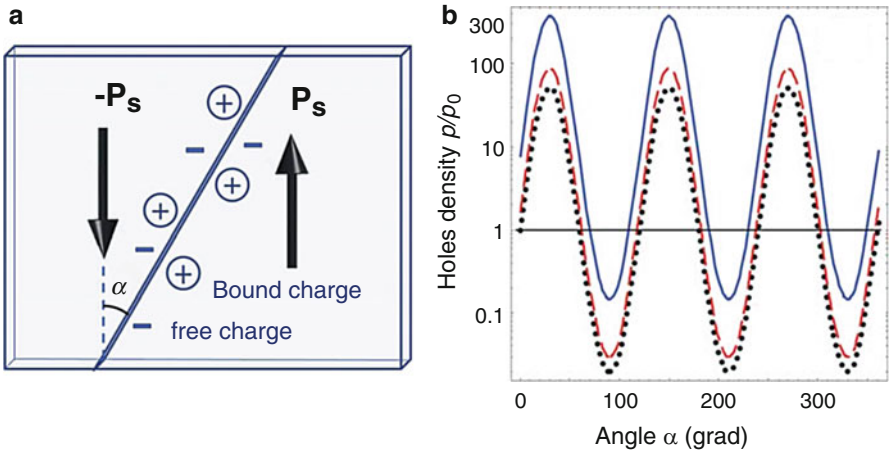

Fig. 20 (**a**) Schematic of a charged domain wall (Reproduced from [44]. © IOP Publishing Ltd. All rights reserved.) (**b**) Relative hole density at different rotation angles in uncharged 180° domain walls in multiferroic $BiFeO_3$. Black-dotted curves are calculated without deformation potential $\Xi_{ij}^p = 0$ and flexoelectric coupling $f_{ij} = 0$. Solid curves are calculated for different coefficients: $f_{11} = -1.38 \times 10^{-11}\mathrm{C}^{-1}\mathrm{m}^{-3}$, $f_{12} = 0.67 \times 10^{-11}\mathrm{C}^{-1}\mathrm{m}^{-3}$, $f_{44} = 0.85 \times 10^{-11}\mathrm{C}^{-1}\mathrm{m}^{-3}$, and $\Xi_{ij}^p = 0$ (*red solid curves*); $2f_{ij}$ and $\Xi_{ij}^p = 21$ eV (*magenta solid curves*); $3f_{ij}$ and $\Xi_{ij}^p = 21$ eV (*blue solid curves*) (Reprinted with permission from [45]. Copyright (2012) American Physical Society)

deformations through two mechanisms, i.e., the so-called deformation potential and the flexoelectric coupling (flexoelectric field in ferroelectric domain walls and flexo-roto field in twin walls). Figure 20b shows the influence of flexoelectric coupling on the hole density of the uncharged 180° domain wall in $BiFeO_3$, with different flexoelectric coefficients and rotation angles. One can see that the variations of hole density was about one order of magnitude, depending on the strength of flexoelectric coupling. The anisotropy of the hole density was attributed to the angle-dependent electrostriction. Furthermore, the conductivity of charged domain walls has also been demonstrated to be modified by flexoelectricity.

5 Applications of Flexoelectric Effect

Being a commonly existing electromechanical coupling effect, flexoelectric effect provides us more possibilities to meet the urging need for new design and fabrication of nanodevices. The first potential application of flexoelectric effect resides in the so-called pseudo-piezoelectric composites. As discussed before, flexoelectricity is a universal mechanism in materials with any symmetry, so it can still induce polarizations in non-piezoelectric materials by inhomogeneous deformation. This effect largely broadens the candidate materials for piezoelectric devices, which can be lead-free, biocompatible, and even flexible. Fousek [8] first proposed the idea to design piezoelectric composites with non-piezoelectric components. This flexoelectric-type piezoelectric composites were realized by a simple design shown in Fig. 21a. The composites contain an active flexoelectric phase with truncated pyramid shape and a second dielectric phase (air here). When the composites are sandwiched by electrodes and compressed homogeneously, the induced strains in the pyramids are inhomogeneous and result in polarizations by flexoelectricity. Thus the composites exhibit piezoelectric responses.

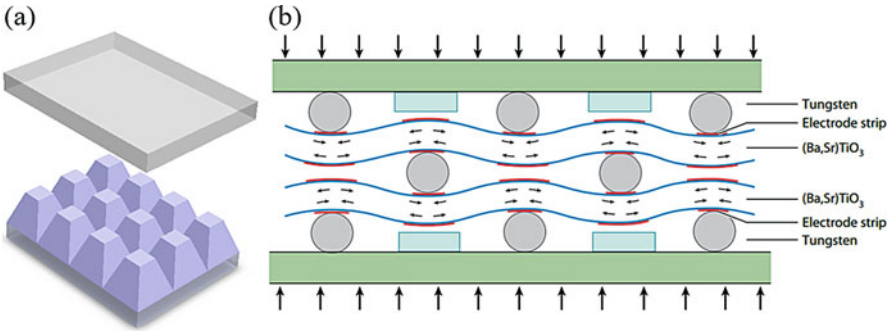

Fig. 21 Schematics of pseudo-piezoelectric composites. (**a**) The design with truncated pyramid array (Reprinted from [46], Copyright (2013), with permission from Elsevier.). (**b**) The design employing transverse flexoelectricity (Reprinted with permission from [47]. Copyright (2009) AIP Publishing LLC.

An imaginative design to employ the large transverse flexoelectricity of BST is illustrated in Fig. 21b. The homogeneous compression leads to the bending of the paraelectric BST layers and results in charge separations by flexoelectricity. Metallic stripes are placed at positions with maximum strain gradients to collect the induced charges. An effective piezoelectric coefficients is reported to be higher than 4300 pC/N for a six-unit three-layer composite. It should be noted that the converse piezoelectric effect in this structure is weak due to the relative homogeneity of electric field between the parallel strips. This separate control of direct and converse piezoelectric effect is favorable for applications requiring sensing but not actuating and vice versa. Theoretical analysis on pseudo-piezoelectric composites has been conducted. Various applications of the pseudo-piezoelectric composites, such as sensors, actuators, transducers, energy harvesters, and nanogenerators, were also reported.

The interaction between flexoelectricity and piezoelectricity can also lead to a novel nanoscale ferroelectric device, i.e., strain diode, as illustrated in Fig. 22. The cantilever is a buffered sandwich structure with a (110)-oriented PZT active layer as the core, STO as electrodes, and yttria-stabilized zirconia (YSZ) as the bottom buffer. When the top surface is exerted to a voltage, negative for example, the bending curvature of the cantilever will be large or small, depending on the ferroelectric polarization directions in the PZT layer. If the polarization is upward, the negative voltage of the top surface will increase the polarization, which leads to an out-of-plane (parallel to the polarization direction) expansion and an in-plane contraction due to electrostriction. Thus an upward bend of the cantilever occurs by the constraint of the buffer. Meanwhile, for downward polarization, the voltage will cause an out-of-plane contraction and in-plane expansion, which leads to a downward bend of the cantilever. On the contrary, the voltage-induced bending by flexoelectricity is independent with the polarization directions, which is always upward because of the negative flexoelectric coefficients for (110)-oriented perovskites. Therefore, for upward polarization, both piezoelectricity and flexoelectricity

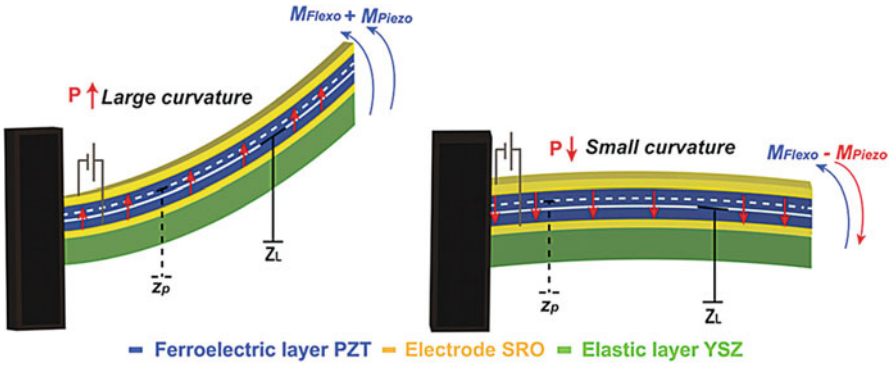

Fig. 22 Schematic illustration of the strain diode, which is attributed to the enhancement and suppression of flexoelectricity on piezoelectric response. Reproduced from [48] with permission of The Royal Society of Chemistry

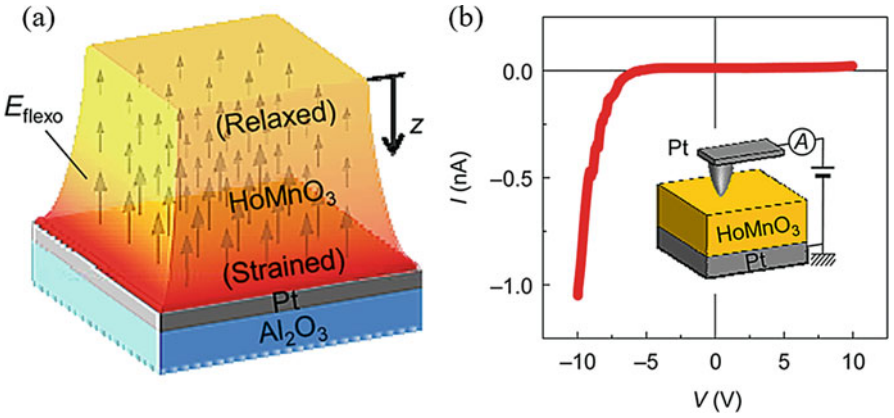

Fig. 23 (**a**) Schematic of strain relaxation and the associated flexoelectric field in an epitaxial $HoMnO_3$ film grown on Pt(111)/Al_2O_3(0001) substrate. (**b**) The *I-V* curve of such a film which shows a rectifying diode effect. Reprinted with permission from [49]. Copyright (2012) American Chemical Society

favor the upward bending and cause a large curvature. In contrast, for downward polarization, the direction of the bending caused by piezoelectricity and flexoelectricity is opposite, which leads to a smaller curvature. A two-state strain diode is thus obtained.

Besides strain diode, flexoelectricity can also lead to an electrical diode, as reported by Lee et al. [49]. For epitaxial $HoMnO_3$ film grown on Pt(111)/Al_2O_3(0001) substrate, as shown in Fig. 23a, the misfit strain is as high as +3.5%. The flexoelectric field due to strain relaxation is estimated to be $E_s \geq 10$ MVm^{-1}, which is comparable to the electric field in conventional *p-n* junctions. The flexoelectric field-induced polarization causes the positive bound charge at top of the $HoMnO_3$/Pt interface and negative bound charge at bottom of the interface. These bound charge would result in a high Schottky barrier at the interface. Due to the small barrier height at surface, electrons are more likely to be injected there and result in a rectifying diode effect, as the *I-V* curve shown in Fig. 23b.

Another promising application of flexoelectricity is the nonvolatile ferroelectric memories with the ferroelectric domains written and erased through mechanical loads. The mechanism has been discussed in Sect 4.3.1. The typical mechanical writing and electrical reading process using an AFM tip is illustrated in Fig. 24. Without applying an external electric field, mechanical writing/erasing of ferroelectric domain can avoid the associated dielectric breakdown and current leakage problem, so it is promising for application in nonvolatile ferroelectric memory with ultrahigh data storage density and less power consumption. One of the challenges of such an application is that mechanical switching reported in ferroelectric film so far is unidirectional, as the strain gradient is fixed in direction.

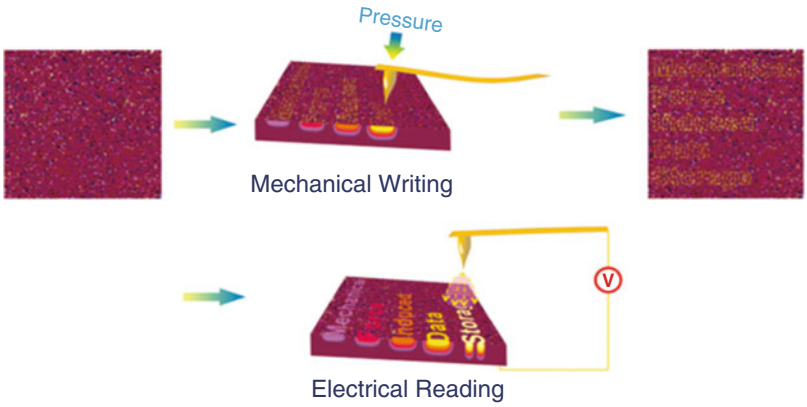

Fig. 24 Schematic illustration of the mechanical writing and electrical reading on ferroelectric thin film by AFM tip. Reprinted with permission from [50]. Copyright (2015) AIP Publishing LLC

6 Summary

In this chapter, we have presented a review on the recent progress of flexoelectricity at the nanoscale, with emphasis on a special class of materials, namely, ferroelectrics. Flexoelectricity is a universal electromechanical coupling effect between polarization and strain gradients and between strain and polarization gradients. Due to its size-dependent behavior, flexoelectricity plays a significant role at the nanoscale. It can influence the dielectric and electromechanical responses of materials, generate imprint behaviors in ferroelectric nanofilms, and affect the global and local characteristics of nanodomains and domain walls. It is promising to utilize flexoelectric effect in potential applications on micro-nano electromechanical systems, such as pseudo-piezoelectric composites, diodes, and nonvolatile ferroelectric memories.

It is noteworthy that there still exist some confusable issues in this rapid growing field. Flexoelectric coefficients, which characterize the significance of flexoelectricity, exhibit large discrepancies in their magnitudes between theoretical calculations and experimental measurements. Meanwhile, the available database of flexoelectric coefficients is also limited. Consequently, there are difficulties in assessing the role of flexoelectricity in novel phenomena, in predicting undiscovered behaviors of flexoelectricity by theoretical modeling and simulations, and in precise design of nanodevices based on flexoelectricity. To solve this problem, both the experimental methods and theories of flexoelectricity need to be further developed. The techniques of employing flexoelectricity, such as strain gradient engineering, are also awaiting to be further explored. Though challenging, it is believed that the progress of flexoelectricity in the near future will bring us more possibilities.

References

1. Mashkevich VS, Tolpygo KB. Electrical, optical and elastic properties of diamond typer crystals. 1. Sov Phys JETP-USSR. 1957;5(3):435–439.
2. Kogan SM. Piezoelectric effect during inhomogeneous deformation and acoustic scattering of carriers in crystals. Sov. Phys. Solid State. 1964;5(10):2069–70.
3. Mindlin RD. Polarization gradient in elastic dielectrics. Int. J. Solids Struct. 1968;4(6):637-642.
4. Bursian EV, Zaikovsk OI. Changes in curvature of a ferroelectric film due to polarization. Sov Phys Solid State USSR. 1968;10(5):1121.
5. Bursian EV, Trunov NN. Nonlocal piezo-effect. Fizika Tverdogo Tela. 1974;16(4):1187–90.
6. Indenbom VL, Loginov EB, Osipov MA. Flexoelectric effect and crystal-structure. Kristallografiya. 1981;26(6):1157–62.
7. Tagantsev AK. A theory of the flexoelectric effect in crystals. Zhurnal Eksperimentalnoi i Teoreticheskoi Fiziki. 1985;88:2108–22.
8. Fousek J, Cross LE, Litvin DB. Possible piezoelectric composites based on the flexoelectric effect. Mater. Lett. 1999;39(5):287–91.
9. Ma W, Cross LE. Observation of the flexoelectric effect in relaxor Pb ($Mg_{1/3}Nb_{2/3}$) O_3 ceramics. Appl. Phys. Lett. 2001;78(19):2920–1.
10. Zubko P, Catalan G, Buckley A, Welche PRL, Scott JF. Strain-gradient-induced polarization in $SrTiO_3$ single crystals. Phys. Rev. Lett. 2007;99(16):67601. Erratum in Physical Review Letters. 2008; 100(19):199906
11. Li HF, Zhang GH, Zheng Y, Wang B, Chen WJ. Ab initio study on mechanical-bending-induced ferroelectric phase transition in ultrathin perovskite nanobelts. Acta Mater. 2014;76:472–81.
12. Resta R. Towards a bulk theory of flexoelectricity. Phys. Rev. Lett. 2010;105(12):127601.
13. Maranganti R, Sharma P. Atomistic determination of flexoelectric properties of crystalline dielectrics. Phys. Rev. B. 2009;80(5):054109.
14. Hong J, Catalan G, Scott JF, Artacho E. The flexoelectricity of barium and strontium titanates from first principles. J. Phys. Condens. Matter. 2010;22(11):112201.
15. Hong J, Vanderbilt D. First-principles theory of frozen-ion flexoelectricity. Phys. Rev. B. 2011;84(18):180101.
16. Hong J, Vanderbilt D. First-principles theory and calculation of flexoelectricity. Phys. Rev. B. 2013;88(17):174107.
17. Ponomareva I, Tagantsev AK, Bellaiche L. Finite-temperature flexoelectricity in ferroelectric thin films from first principles. Phys. Rev. B. 2012;85(10):104101.
18. Stengel M. Unified ab initio formulation of flexoelectricity and strain-gradient elasticity. Phys. Rev. B. 2016;93(24):245107.
19. Yudin PV, Ahluwalia R, Tagantsev AK. Upper bounds for flexoelectric coefficients in ferroelectrics. Appl. Phys. Lett. 2014;104(8):082913.
20. Majdoub MS, Sharma P, Cagin T. Enhanced size-dependent piezoelectricity and elasticity in nanostructures due to the flexoelectric effect. Phys. Rev. B. 2008;77(12):125424.
21. Majdoub MS, Sharma P, Çağin T. Dramatic enhancement in energy harvesting for a narrow range of dimensions in piezoelectric nanostructures. Phys. Rev. B. 2008;78(12):121407.
22. Chen J. Micropolar theory of flexoelectricity. J Adv. Math. Appl. 2012;1(2):269–74.
23. Henmi N, Tohyama M. Measurement of Flexoelectric Effect in Lead Zirconate Titanate Ceramics. J. Adv. Mech. Des. Syst. Manuf. 2011;5(1):1–6.
24. Cross LE. Flexoelectric effects: Charge separation in insulating solids subjected to elastic strain gradients. J. Mater. Sci. 2006;41(1):53–63.
25. Ma W, Cross LE. Flexoelectric polarization of barium strontium titanate in the paraelectric state. Appl. Phys. Lett. 2002;81:3440–2.
26. Ma W, Cross LE. Strain-gradient-induced electric polarization in lead zirconate titanate ceramics. Appl. Phys. Lett. 2003;82(19):3293–5.
27. Narvaez J, Saremi S, Hong J, Stengel M, Catalan G. Large flexoelectric anisotropy in paraelectric barium titanate. Phys. Rev. Lett. 2015;115(3):037601.

28. Sinnamon LJ, Bowman RM, Gregg JM. Thickness-induced stabilization of ferroelectricity in $SrRuO_3/Ba_{0.5}Sr_{0.5}TiO_3$/Au thin film capacitors. Appl. Phys. Lett. 2002;81(5):889–91.
29. Catalan G, Noheda B, McAneney J, Sinnamon LJ, Gregg JM. Strain gradients in epitaxial ferroelectrics. Phys. Rev. B. 2005;72(2):020102.
30. Gharbi M, Sun ZH, Sharma P, White K. The origins of electromechanical indentation size effect in ferroelectrics. Appl. Phys. Lett. 2009;95(14):142901.
31. Liang X, Yang W, Hu S, Shen S. Buckling and vibration of flexoelectric nanofilms subjected to mechanical loads. J. Phys. D. Appl. Phys. 2016;49(11):115307.
32. Chen WJ, Zheng Y, Luo X, Wang B, Woo CH. Ab initio study on the size effect of symmetric and asymmetric ferroelectric tunnel junctions: A comprehensive picture with regard to the details of electrode/ferroelectric interfaces. J. Appl. Phys. 2013;114(6):064105.
33. Tagantsev AK, Gerra G. Interface-induced phenomena in polarization response of ferroelectric thin films. J. Appl. Phys. 2006;100(5):051607.
34. Gruverman A, Rodriguez BJ, Kingon AI, Nemanich RJ, Tagantsev AK, Cross JS, et al. Mechanical stress effect on imprint behavior of integrated ferroelectric capacitors. Appl. Phys. Lett. 2003;83(4):728–30.
35. Lu H, Bark CW, De Los Ojos DE, Alcala J, Eom CB, Catalan G, et al. Mechanical writing of ferroelectric polarization. Science. 2012;336(6077):59–61.
36. Chen WJ, Zheng Y, Xiong WM, Feng X, Wang B, Wang Y. Effect of mechanical loads on stability of nanodomains in ferroelectric ultrathin films: Towards flexible erasing of the non-volatile memories. Sci. Rep. 2014;4
37. Lee D, Yoon A, Jang SY, Yoon JG, Chung JS, Kim M, et al. Giant flexoelectric effect in ferroelectric epitaxial thin films. Phys. Rev. Lett. 2011;107(5):057602.
38. Catalan G, Lubk A, Vlooswijk AHG, Snoeck E, Magen C, Janssens A, et al. Flexoelectric rotation of polarization in ferroelectric thin films. Nat. Mater. 2011;10(12):963–7.
39. Ahluwalia R, Tagantsev AK, Yudin P, Setter N, Ng N, Srolovitz DJ. Influence of flexoelectric coupling on domain patterns in ferroelectrics. Phys. Rev. B. 2014;89(17):174105.
40. Chen WJ, Zheng Y, Wang B. Vortex domain structure in ferroelectric nanoplatelets and control of its transformation by mechanical load. Sci. Rep. 2012;2:796.
41. Chen W, Zheng Y, Feng X, Wang B. Utilizing mechanical loads and flexoelectricity to induce and control complicated evolution of domain patterns in ferroelectric nanofilms. J. Mech. Phys Solids. 2015;79:108–33.
42. Gu Y, Li M, Morozovska AN, Wang Y, Eliseev EA, Gopalan V, Chen LQ. Flexoelectricity and ferroelectric domain wall structures: Phase-field modeling and DFT calculations. Phys. Rev. B. 2014;89(17):174111.
43. Morozovska AN, Eliseev EA, Glinchuk MD, Chen LQ, Gopalan V. Interfacial polarization and pyroelectricity in antiferrodistortive structures induced by a flexoelectric effect and rotostriction. Phys. Rev. B. 2012;85(9):094107.
44. Yudin PV, Tagantsev AK. Fundamentals of flexoelectricity in solids. Nanotechnology. 2013;24 (43):432001.
45. Morozovska AN, Vasudevan RK, Maksymovych P, Kalinin SV, Eliseev EA. Anisotropic conductivity of uncharged domain walls in $BiFeO_3$. Phys. Rev. B. 2012;86(8):085315.
46. Jiang X, Huang W, Zhang S. Flexoelectric nano-generator: Materials, structures and devices. Nano Energy. 2013;2(6):1079–92.
47. Chu B, Zhu W, Li N, Cross LE. Flexure mode flexoelectric piezoelectric composites. J. Appl. Phys. 2009;106(10):104109.
48. Bhaskar UK, Banerjee N, Abdollahi A, Solanas E, Rijnders G, Catalan G, Flexoelectric MEMS: towards an electromechanical strain diode. Nanoscale. 2016;8(3):1293–8.
49. Lee D, Yang SM, Yoon JG, Noh TW. Flexoelectric rectification of charge transport in strain-graded dielectrics. Nano Lett. 2012;12(12):6436–40.
50. Chen X, Tang X, Chen XZ, Chen YL, Guo X, Ge HX, et al. Nonvolatile data storage using mechanical force-induced polarization switching in ferroelectric polymer. Appl. Phys. Lett. 2015;106(4):042903.